Universitetet i Stavanger

STUDENT: ELIN HERREDSVELA & STIG ROAR L. RØDNE
VEILEDER: SUDATH C. SIRIWARDANE & FREDRIK BJØRHEIM

Structural Integrity of Flange Connection in Onshore Wind Turbine Towers.

Investigating Premature Bolt Failures

Bachelor Thesis 2024

Civil Engineering / Structural engineering

Civil Engineering

Faculty of science and engineering

Acknowledgments

This theisis could not have been completed without the assistance of too many in this university to name. Our thanks go to the two supervisors of our thesis, Sudath C. Siriwardane, Professor of Structural Engineering, and Fredrik Bjørheim, Associate Professor of Structural Engineering. Their encouragement and unwavering support have helped us all the way on this journey.

We would like to thank the team in the workshop and laboratory for their marvellous help. Special thanks go out to Are Molund, Kjell Høgemark, Caroline Einvik and the outstanding laboratory team: Johan A. Thorkaas, Engineer-in-charge; Mats Ingdal, Senior Engineer; and Espen Undheim, Senior Engineer. They have been of particular value to our research through their help with sample preparation, testing and discussions of results.

A very special thanks are due to the CEO of G2MT's laboratory in Houston, Texas, Mrs. Angelique Lasseigne, for her knowledge and time dedicated to reviewing our ideas and indicating what course they should take.

We never would have gotten this far without the support and direction of the whole lot of you. Also, we would like to thank our families who have, by their encouragement and example, given us enormous energy to finish this thesis.

Thank all mentioned and unmentioned people who accompanied us in our academic journey!

With thousand thanks,

Elin Herredsvela & Stig Roar Rødne

Abstract

Premature bolt failure on onshore wind turbine towers is a major issue and hamper field operation safety. As such, this article examines the structural integrity of 32CrB4 steel M56 high strength grade 10.9 flange connection bolts as applied on wind turbine towers. By comprehensively analyzing characteristics like mechanical properties, chemistry and microstructure, this study hopes to point out what is behind the failure of these bolts.

A range of testing was utilized to determine the strength and ductility of these bolts. Analysis of the chemical composition conducted with scanning electron microscopy and energy dispersive spectroscopy--found elemental distributions that could affect material performance. Tests that revealed defects or inconsistencies were performed using optical microscopy, scanning electron microscopy, and electron backscatter detection.

This showed that while the bolts met their mechanical requirements, there were aspects which might indicate hydrogen embrittlement. These include intergranular cracking near the edges of the fracture surface on all of the bolts. In addition, the variations in size and distribution of gaps (especially one test piece) indicated weakness.

In spite of these findings, it has not yet been possible to pin down the cause or causes of bolt failures conclusively due to limitations inherent in the data as well as the complex interplay between different mechanisms leading to failure. This study underscores the urgent need to execute further research in this area to understand all factors affecting the fracture in theese bolts. By providing interesting parties in the wind turbine industry insights that they can use to develop more efficient strategies for maintenance and ultimately make turbine maintenance safer and more stable.

Abbreviations

EAC – Environmentally assisted cracking

HE - Hydrogen embrittlement

OD - Outer Diameter

1. Introduction

1.1. Background and motivation.

Wind turbines form an integral part of our ever increasing demand for renewable energy, supplying large quantities of power without any of the greenhouse gases associated with fossil fuels

These structures are specifically designed to endure considerable mechanical loads from rotational forces and various wind speeds [1]. A critical concern regarding structural integrity is the tower-tower bolts: bolt failures continue to be a significant problem even though technology has led to an increase in turbine efficiency and its durability. Such failures may result in production reduction, safety hazards and expensive repairs.

These errors in bolt integrity can be attributed to fatigue caused by cyclical loading, corrosion from the environment, improper assembly and production defects [2, 3]. The repercussions range from minor losses of efficiency because components are not aligned as they should be to catastrophes where human beings are injured and the environment damaged in a major way.
This project was heavily sparked by one student's connection to the wind turbines in question, which lent a personal interest to determine what was causing these bolt failures. This unique viewpoint underscores the pressing need for a scientific exploration into the material science of turbine bolts for increasing both turbine safety and its dependability because this is often overlooked in maintenance strategies.

This investigation focus on three bolts from a wind turbine in Scandinavia. These bolts, of dimension M56 and quality 10.9, following UNE-EN-ISO 898-1 [4] and UNE-EN- ISO 898-2 [5] and design, dimensions, and specifications of high- strength hexagon head bolts are defined by DIN 6914 [6]. The bolts have been in service for approximately two years, tightened by two stage tightening to where max is 1000 Nm. The bolts have been securing tower- tower flange connections within the turbine structure.

All three bolts are from the same batch, these bolts are made of 32CrB4 steel, which is known for its tempered martensite structure that promises both strength and durability [7].

Detailed chemical composition, presented in the steel manufacturer's Mill Test Certificate [22], is crucial to reflect on the bolts' performance under operational tensions, Table 1.

Table 1 Chemical composition of bolts [22].

Element	Percentage %
C	0.330
Mn	0.820
Si	0.240
P	0.010
S	0.007
Cr	1.180
Ni	0.790
Cu	0.070
Al	0.027
Ti	0.0460
B	0.0032
H	0.00012

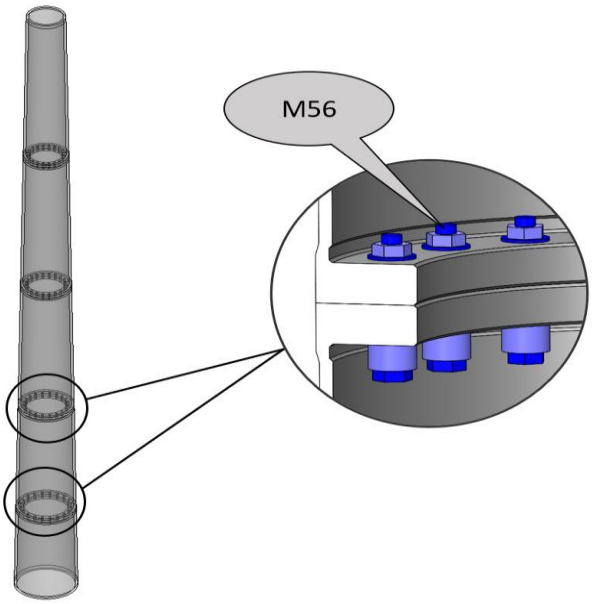

Figure 1 Visualization of locations of M56 bolts in wind turbine tower.

1.2. Aims and objectives.

The aim of this thesis is to explore the reasons for bolt failures in onshore wind turbines and propose strategies to prevent these failures. The thesis focuses on a number of narrow targets:

Classification and Evaluation of the Mechanical Strength of Bolts: This part will put the wind turbine bolts tensile strength, impact ductility, toughness properties through tests, such as Charpy, tensile and hardness to find their mechanical properties.

Chemical Analysis of Composition: A detailed study is carried out in order to identify the presence in bolt material of elements that could weaken it. Techniques to be used include scanning electron microscopy (SEM) with EDS, which will determine the percentage of atoms in each element; experimental chemistry that may have been done on an integrated

circuit and so forth.

Microstructure Inspection: By means of SEM and optical microscopy, the focus is placed on the micro structure of these bolts in an effort to turn up micro structural defects or anomalies such as grain boundary brittleness, phases, or inclusions which will affect its mechanical integrity.

1.3. Importance of this research

This thesis is designed to expound the things that may lead to the failure of bolts in wind turbines onshore, in an effort to aid future research as well I's just an exploration.
Though it is exploratory research, the authors expect that it may yield critical findings directly related to questions that concern fastener integrity. Stakeholders in the wind industry could benefit from this.

The investigation focus on the mechanical properties, chemical composition, and microstructures of turbine bolts. Identifying trends or any susceptibility may offer bolt manufacturers needed feedback about the effectiveness of their present materials and design processes.

Wind-farm investors and operators who understand the underlying reasons for bolt failures stand to profit greatly from this research. Knowledge of what causes these failures could lead to better maintenance plans and more thought-through maintenance strategies, helping to minimize downtimes and increase working efficiency. This could yield cost savings and more electrical output, thus promoting the overall profitability and sustainability of the individual wind farm.

Also, the information in this study could also help steer future procurement decisions and harder guidelines for quality assurance. Using precise recommendations based on this data, the study aims to move turbine operations closer to safer and more dependable standards in wind industry.

1.4. Limitation

All should be conducted under constraints, and that has shaped this thesis scope and output significantly. Being civil engineering students with very little to non background in material science and mechanical engineering has meant a steep learning curve. Consequently, there is also less depth of analysis possible.

Technical issues with equipment at the university have sometimes impeded experimental work--affecting data collection and analysis; There is also a lack of detailed industrial data for bolt failures due to confidentiality. It is therefore not possible to analyze several aspects deeply.
In addition, material composition and properties of bolts as delivered by the manufacturer simply cannot be compared: This not only severely restricts understanding of potential material deficiencies; it also restricts direct comparison with industry standards, or any other materials used in similar applications.
As a result it is also impossible to know whether any such correspondence exists.
Limited availability of additional bolt materials and lack of non-fractured bolts made it impossible to investigate bolt conditions prior to bolt fracture.

These limitations are essential for the understanding of boundaries that have formed this thesis and its results.

2. Literature Review

2.1 Manufacturing

To ensure bolts integrity and reliability, it is very necessary to understand in general terms just what is involved in manufacturing them. Each individual process step in bolt manufacturing aims at some improvement of the material's mechanical properties and durability in manufacture. When the manufacturer of the bolts under consideration was asked what process actually, they described it briefly in a mail response [8];

Manufacturers 'Production Process:
The manufacturer clarified several points of note in its production process:

Surface treatment: Sand-blasting not acid washing The bolts are not washed in acid, but sandblasted. This method has been found to be superior because it does not release hydrogen into the steel which might then give rise to hydrogen embrittlement. [8]

Hydrogen Control: The manufacturer has very strict maximum limits on the hydrogen content in their steel [8].

Galvanizing Process: Hot-dip galvanization is used to coat the bolts (tZN/HDG/fzv), not zinc electro plating. By coating bolts in molten zinc from hot-dip galvanizing offers excellent corrosion resistance while avoiding the problems of hydrogen embrittlement associated with zinc electro plating. [8]

Potential Hydrogen Introduction: While the manufacturer guarantees minimal hydrogen content during production, they also admit that hydrogen could be introduced at any stage, whether during production, assembly or even after installation [8]. They point out the importance of handling and environmental conditions as well as lifecycle management for bolts.

Detailed Manufacturing Steps:

Hot Forging [8]: Heat steel into shape Hot forging changes both the microstructure and grain structure. This makes it much stronger than if it were built with cold working methods that give little change to either structure, thus increased toughness but at a corresponding loss of ductility [9].

Hardening [8]: The bolts are sent back through a heat treatment again, raising their hardness. This means heating the bolts to high temperatures and then rapidly cooling in oil (quenching) until desired mechanical properties have been achieved [10].

Hardening Control [8]: Whether, after the above hardening process, the bolts have achieved hardness and mechanical properties designed to meet specifications must be verified. This step in quality control is essential in order maintain uniformity and reliability of the bolts' performance [11].

Hot-Dip Galvanizing [8]: After cleaning and hardening, the bolts are immersed in molten zink to put a coating on them. This extends their use under most corrosive environment. The process offers outstanding corrosion resistance [12].

Inspection [8]: After galvanization, the bolts go through inspection and various examinations to make sure that the spread of the coating is even and that it adheres well [11].

Packaging [8]: As a final step, bolts are packed, stored or shipped to client [11].

2.1.1. Common Bolt Failures

Understanding the reasons for bolt failure is essential for improving the safety and reliability of engineering structures. Bolt failures can lead to significant human dangers, economic losses as well as unavailability of services. Despite in-depth research, but still the real causes

of bolt failure are not easy to detect [2]. This section briefly introduces the most common causes of bolt failure, presents multiple scientific perspectives, and emphasizes that details often are not well-documented [2].

Table 2 Reproduction from [13]: Common bolt failures.

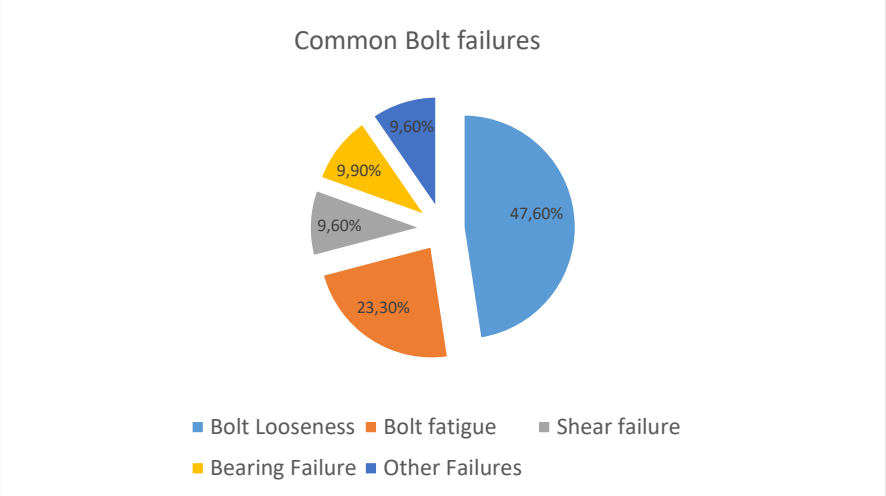

From an initial detection through different sources, including a Bolt Science Newsletter statistical survey [13] and analysis of bolt incidents in the petroleum industry [2], the common causes for bolt failure can be grouped as:

Insufficient preloading and self-loosening of bolts: Insufficient preloading is the most common cause of bolt failure, leading to self-loosening. When preload is insufficient, the bolted joint may separate under axial loads, producing high alternating stresses that make bolt fatigue happen. In friction grip shear loaded applications joint slip due to lack of preload can cause bending and ultimately fatigue failure of the bolts. However, locking devices will stop self-loosening but not the resulting fatigue caused by repeated loading cycles which lead to joint slip [13].

Fatigue failures: Fatigue is the single greatest cause of bolt failure and usually associated with low preload levels. In friction grip joints, bolt fatigue occurs whenever joint slip induces bending stress for a bolt. Initiation and development of fatigue failure is clear this way. If bolts are torsion tested to destruction in the Junker test for any locked they can lose after

several thousand cycles due simply to fatigue, emphasizing how important it is that they be kept up with preloading so they don't come loose [13].

Shear Failure: Shear failure of bolt includes thread shear and direct shear. Thread shear means the threads are sheared off. This may happen in a tapped hole when there isn't enough depth of engagement. It is also referred to as thread stripping. Direct shear involves the breaking of the bolt itself into halves or pieces. Under most conditions, this type does not occur for mechanical components which rely heavily on friction grip joints, where shear is transmitted across an interface area at the joint rather than straight through the bolt. Nevertheless, it sometimes still causes catastrophic structural failures [13].

Bearing Failure: When a mounting hole fails, debris from the hole crushes or extrudes around its perimeter into material which then hardens in an unnatural manner. This leads to group movement and ultimately bolting failure [2].

Hydrogen Embrittlement: Hydrogen embrittlement is a less common but serious cause of bolt failure. When hydrogen atoms infiltrate the microstructure of a bolt material, they are causing cracks to form. This is particularly troublesome in high-strength bolts of property class 12.9 or in bolts of property class 10.9 and may arise from manufacturing processes such a electroplating or environmental conditions such as corrosion [2, 13].

Composite Excitation Failures: Research has shown that when composite excitation is applied simultaneously to bolts—i.e., both axial and transverse loads—it becomes a competitive failure mode between loosening and fatigue. Transverse loads cause bolt-loosening, and axial loads cause fatigue damage. The combination of these two loads greatly reduces bolt life. The transverse-to-axial load ratio (ξ) affects which failure mode predominates. A high ξ ratio means that most of the failures will be loosening, while a low ξ ratio is linked to fatigue [15].

Fracture Mechanics and Material Performance: Based on Callisters [16], the inability to establish the choice of a material correctly, improper processing, or misuse is often the reason for product failure. Fundamentals of fracture mechanics teaches us that a property which influences the way materials behave under stress is absolutely vital for predicting failure modes. But whether or not it slips into brittle fracture, ductile fracture arises as the material's capacity for plastic deformation is made important. When ductile materials fracture, a great

deal of energy is absorbed before the break occurs; hence there is large deformation of material, while brittles simply shatter [16].

Ductile or Brittle Fracture: At the crack tip, ductile fracture involves considerable plastic deformation and very slowly increased stress. On the other hand, brittle fractures occur without any plastic deformation and spread instantly from the word go. Knowing these principles is indispensable for engineers so as to anticipate possible failures and act on them in advance [16].

To sum up, while bolt loosening and fatigue are the most common failure modes, there are other dangerous fracture modes, such as shear failure or hydrogen embrittlement. A subsequent section will go into fracture mechanics research in more detail.

2.2. Characteristics and Applications of Medium Carbon Steels Enhanced by Alloying.

Medium carbon steel is steel containing carbon between any field between 0,25wt% to 0.60wt%[16]. One such steel named 32CrB with a carbon content of 0.33 wt% is an example of this type, excellent in working under heavy loads such as being in the flange bolts for wind turbines. Ideal performance characteristics make it able to be hot formed or cold without problem. [7] These types of steels usually need some heat treatments to make their mechanical properties meet requirements [16].

Alloying elements such as chromium, molybdenum, nickel and boron are used to perfect the performance of these steels [16]. These alloys yields increased hardenability and improved ability to resist decay by corrosion; nickel brings toughness [16]. Furthermore, even a very small dash of boron, alloy-wise, can significantly better the hardenability, enabling it to meet requirements for uniform properties across thicker sections. This is crucial in fabricating high-strength components such as bolts [7].

However, the hardening process can make the alloy brittle; especially if martensite formation is achieved through rapid quenching [17]. Unlike low-carbon steels, medium-carbon variants with higher tensile strength also have increased rigidity or brittleness. These are properties which are essential to avoid breakage due to impact or shock loads [16]. Methods such as spheriodize annealing--particularly associated with controlled improvement in formability for cold forging--can also be used to get past these problems. These measures ruly are indispensible in other processes seeking a strengthening of ductility [7]. Now in a bolt, a part that faces constant dynamic stress and cannot afford to vary with performance if such annealing operations are not carried out, the metal will not have enough plasticity or toughness to prevent fracture [17].

In summary, medium carbon steel 32CrB, when alloyed with elements like chromium and boron, offers robust solutions [17,16,7].

2.3. Characteristics of martensitic microstructure

When steel is quenched from the austenitizing temperature, which is above the recrystallization point, martensite forms. The rapid cooling transforms austenite's face-centered cubic structure into a body-centered tetragonal structure of martensite. The martensite's carbon content has a major effect on its hardness. This percent can be as high as 0.6 weight. Unlike the strength and hardness of pearlitic steels, which depend largely on microstructural features, for martensite this comes from the effective blocking of dislocation movement by interstitial carbon atoms. This is called solid-solution hardening. Furthermore, martensite has fewer slip systems and so dislocation movement is more difficult, contributing as well to its brittle demeanor. During quenching, the denser austenite is transformed into less dense martensite, creating internal stresses and a net volume increase. These stresses can cause cracking, particularly when the carbon content exceeds 0.5 weight percent [16].

Martensite in its as-quenched state is too brittle and full of internal stresses to be useful in most applications. To remedy these shortcomings and increase the ductility and toughness of martensite, it goes through heat treatment-a process known as tempering. Tempering consists

of heating the quenched martensitic steel to a temperature below copulation, usually between 250°C and 650 °C. This thermal process allows the BCT martensite, a solid solution with respect to carbon, to diffuse its supersaturated carbon and knead it into little islands of cementite (Fe3C). In other words, the single-phase martensitic structure becomes a dual-phase microstructure consisting of ferrite and dispersed particles of fine cementite—tempered martensite. This microstructure is akin to spheroidite but with much smaller and more uniformly distributed cementite particles. The grain boundaries between ferrite and cementite phases act as obstacles to dislocation movement, making strength go up along with happiness while ductility and, to a lesser extent, toughness improve greatly [16]. The dimensions of carbide particles and tempering conditions were more important mechanical issues.

Influenced significantly by the size of cementite particles, the mechanical properties of tempered martensite are influenced strongly as well. This size is governed by tempering temperature and duration. The higher the temperature or longer the tempering time, the larger the cementite particles. The phase boundary area is thus reduced, and its ductility toughness increased at the cost of its softness Conversely, smaller particles because of the greater phase boundary area per unit volume are increased in strength and hardness. Meanwhile the tempering process also plays a critical role in determining the yield and tensile strengths of alloys-in addition to their ductility. But this varies with tempering temperature [16].

While tempering generally improves the toughness of martensite, some steel materials are prone to temper embrittlement, You not as usually called an 'oil treatment ', particularly of artificial alloying elements such as manganese, nickel and chromium, nor those found as residual elements like antimony, arsenic-impurities are phosphorus or tin. This embrittlement occurs when the steel is subjected to tempering in a narrow range of critical temperatures followed by slow-cooling. The embrittled metal will then fracture intergranular along the grain boundaries of the original austenitic phase. In order to prevent tempered embrittlement steels need to be compositionally manageable and tempered outside critical temperature ranges, followed by rapid cooling. Also, by reheating embrittled steels to around 600°C and then quenching below 300°C to Micro å these steels' toughness is substantially restored [16].

2.4. Fracture Mechanics

2.4.1 Ductile Fracture

William and Callister [16] describes simple fracture as follows:

> *"Simple fracture* is the separation of a body into two or more pieces in response to an imposed stress that is static (i.e., constant or slowly changing with time) and at temperatures that are low relative to the melting temperature of the material."

The two main fracture modes for steel are ductile and brittle and the categorization relies on the property for a material to undergo plastic deformation [16]. Fatigue can also be a source to fractures but will not be covered in this thesis.

Ductile metals usually fail due to the results of nucleation and its various stages of growth. Cleavage and intergranular fractures are seen as brittle, but cleavage often coincide with ductile parts of the metals. Ductility is the property for a metal to have undergo plastic deformation [18]. Brittle fractures have to types of fracture, cleavage which is a transgranular fracture and intergranular fracture. The difference is shown in figure 2.

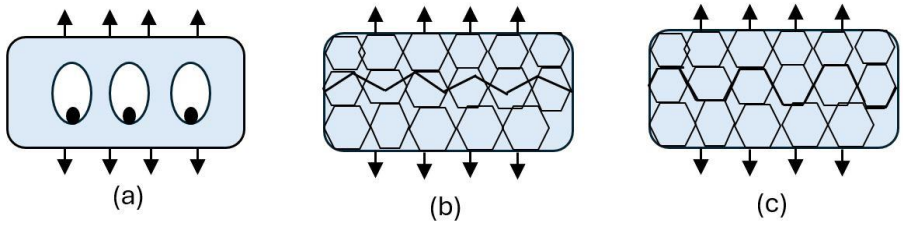

Figure 2 Reproductions from [18, s. 220], "three micro mechanisms of fracture in metals: (a) ductile fracture, (b) cleavage, (c) intergranular fracture."

Ductile growth has various stages and stars with void nucleation, growth, coalescence and ends with possible void coalescence and fracture. In all metals the existence of impurities and second phase particles that are firmly attached in the matrix make possibilities for void nucleation to occur. When the matrix is exposed to sufficient stress the bonds between the particle and matrix breaks and we get void nucleation. Voids will continue to expand and eventually coalesce if plastic strain and hydrostatic stress persist. Should the initial volume of voids be low, less than 10%, then its assumed that each void grow independently. Until further growth makes the voids interact.

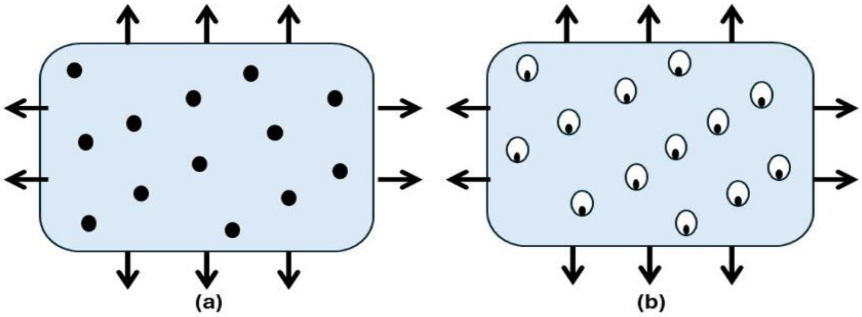

Figure 3 Reproduction from [18, s. 224], "Void nucleation, growth, and coalescence in ductile metals: (a) inclusions in ductile matrix, (b) void nucleation."

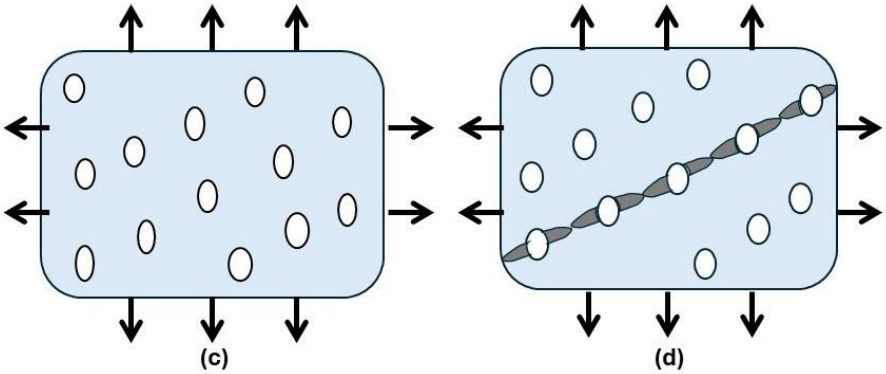

Figure 4 Reproduction from [18, s. 224], "(c) void growth, (d) strain localization between voids."

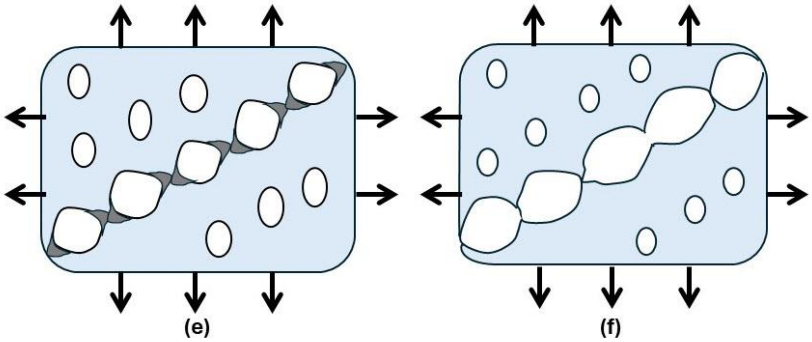

Figure 5 Reproduction from [18, s. 224], "(e) necking between voids, (f) void coalescence and fracture".

According to T.L Anderson we have different continuum models for void nucleation. According to [18] "The Goods and Brown dislocation model, indicates that the local stress concentration increases with decreasing particle size". The Argon et al. being the most used model for void nucleation [18]. They state that, "interfacial stress at a cylindrical particle is approximately equal to the sum of the mean and von mises stress". The combination of these two stresses is defined as the decohesion stress and is defined by [18, s. 219]:

$$\sigma_c = \sigma_e + \sigma_m$$

Equation 1 Decohesion stress.

The effective stress, σ_e, is given by [18, s. 221]:

$$\sigma_e = \frac{1}{\sqrt{2}}\left[(\sigma_1 - \sigma_2)^2 + \left(\sigma_{1-\sigma_3}\right)_+^2(\sigma_3 - \sigma_2)^2\right]^{1/2}$$

Equation 2 Effective Stress in decohesion stress.

Mean stress, σ_m, is defined as [18, s. 221]:

$$\sigma_m = \frac{\sigma_1 + \sigma_2 + \sigma_3}{3}$$

Equation 3 Mean stress.

σ_1, σ_2 and σ_3 are the normal stresses. Argon et. Al model states that when hydrostatic stress increases nucleation strain decreases. Consistence with experimental data it has been seen that void nucleation more often occurs in triaxial tensile stress [18].

As shown in earlier figure 3 to 5. Figure 6 and 7 are from SEM and show dimple fracture surface and microvoid coalescence. According to Anderson [18] dimpled appearance is characteristic of microvoid coalescence.

Kommentert [EH1]: kilde?

Kommentert [EH2]: oppdater

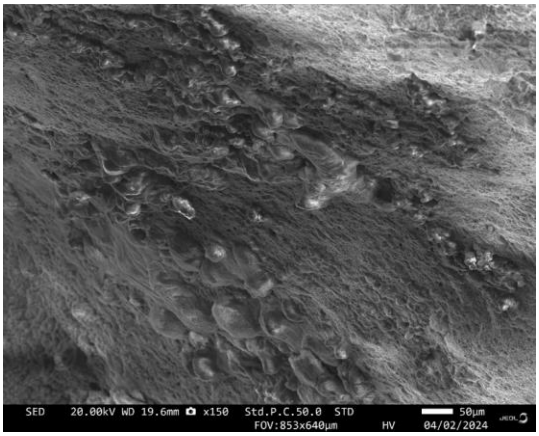

Figure 6 SEM Picture of dimple surface from fracture surface.

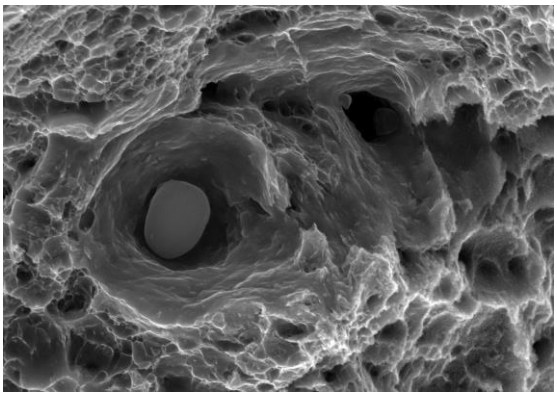

Figure 7 SEM picture microvoid nucleation from FAB-M2 sample.

Cup and cone fracture surfaces are mostly observed in uniaxial tensile tests. This is show in figure 8. In the central region of the specimen, void nucleation and subsequent growth in the larger particles are triggered by the triaxial stress in the neck. With continued strain, the voids coalesce and results in thin and short shaped flaws. Few voids are seen in the outer ring of the sample, this is due to the hydrostatic stress is smaller than in the central region. This defect in the material causes lines of deformation bands to be formed at a 45-degree angle to the direction of stretching. This buildup of strain creates enough plasticity for voids to start forming in the smaller, more numerous particles. Due to these tiny fragments are packed tightly together, instability quickly follows the formation of these smaller voids. Then leading to the complete breakage of the material and giving the matching surfaces a cup and cone shape [18].

Kommentert [EH3]: oppdater

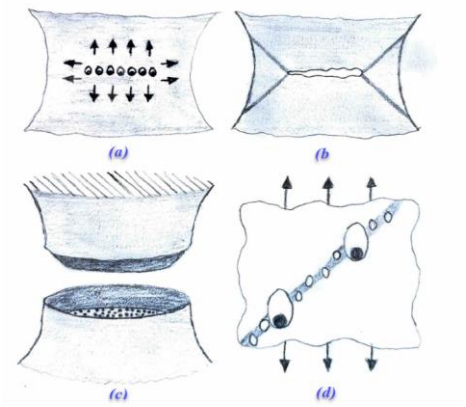

Figure 8 Reproduction from [18, s. 225]: "(a) void growth in a triaxial stress state, (b) crack and deformation band formation, (c) nucleation at smaller particles along the deformation bands, and (d) cup and cone fracture."

When the cracked structure is put under load, the local strains and stresses at the tip, gets strong enough nucleate voids will start to form. As the crack gets more rounded, these voids enlarge and will ultimately connect with the main crack. The crack gets larger as this process keeps on happening. Figure 9 Reproduced from [18] schematically illustrates: "microvoid initiation, growth, and coalescence at the tip of a preexisting crack."

Kommentert [EH4]: oppdater

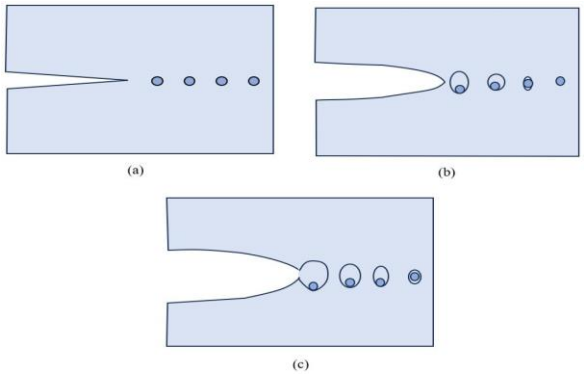

Figure 9 Reproduction from [18, s. 232]: "Mechanism for ductile crack growth: (a) initial state, (b) void growth at the crack tip, and (c) coalescence of voids with the crack tip."

.

2.4.2 Brittle Fracture

According to T.L Andersen [18] “cleavage fracture can be defined as the rapid propagation of a crack along a particular crystallographic plane. It may be brittle in local scale but also be preceded by large-scale plastic flow and ductile growth”. Cleavage fracture is trans granular as shown in Figure 1 (b) and favored cleavage planes have the lowest packing density. This due to less bonds that must be broken the distance between the planes are bigger. At every new grain boundary crossing it changes direction, due to the random orientation of the subsequent grains. T.L Andersen [18] states that: “FCC metals are not vulnerable to cleavage as there are ample slip systems for ductile behavior at all temperatures.” BCC metals don’t have active slip systems and therefore can fail by cleavage at low temperatures. BCC crystal matrix has a ductile-brittle transition when the temperature drops. Since at high temperatures ductile fracture is dominant and at low temperatures cleavage occurs. A multifaceted surface is common on cleavage in a polycrystalline material. Also typical are the “river pattern” on each facet [18]. Figure 10 is an good example of ductile and brittle transition, with both cracks.

Kommentert [EH5]: oppdater

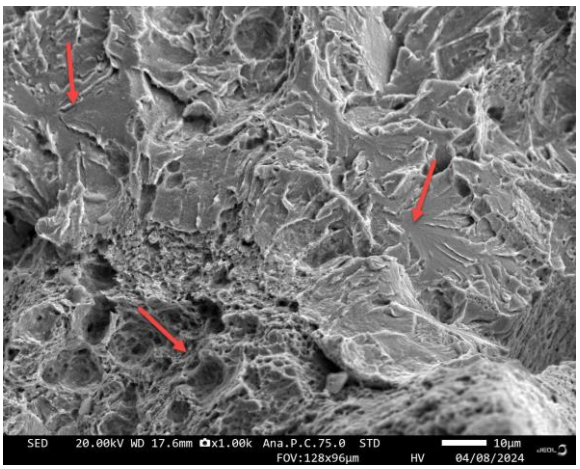

Figure 10 Cleavage fracture with river patterns.

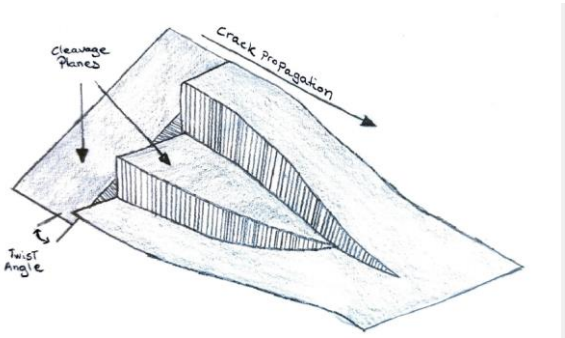

Figure 11 Reproduction from [18, s. 236]: "formation of river patterns, as a result of a cleavage crack crossing a twist boundary between grains."

Figure 11 illustrates the formation of river patterns. When a propagating cleavage crack reaches a grain boundary, it encounters an adjacent grain where the nearest cleavage plane has an angle that is at a tiny twist from the present cleavage plane. This twist mismatch is solved by forming several parallel planes [18].

Kommentert [EH6]: oppdater

According to T.L Anderson [18] "cleavage involves breaking bonds and therefore the local stress must be sufficient to overcome the cohesive strength of the material." The theoretical fracture strength of a crystalline solid is approximately $\frac{E}{\pi}$. However, stress and strain in front of a blunted crack tip, simulated with FEA, shows that at the crack tip the stress achieved ahead is three to four times the yield strength. A macroscopic crack does therefore not induce sufficient stress to exceed the bond strength. A sharp microcrack will ensure enough local stress concentration. In metals the typical mechanism for microcrack formation entails inclusions and second-phase particles [18].

T.L Anderson [18] writes that "the microstructural feature that nucleates cleavage depends on the alloy and heat treatment". Cleavage often starts at the grain boundary carbides in mild steel. Whereas in quenched and tempered alloy steel, its usually either a spherical carbide or and inclusion that has the critical failure. There have been various models regarding the relationship between cleavage fracture stress and microstructure and the majority models ended with an expression similar to the model proposed by Smith, mentioned in [18]. This model for cleavage fracture, defines "stress concentration due to a dislocation pile-up at a grain boundary carbide". Failure criterion is [18, s. 237]:

Kommentert [EH7]: Smith å smith (gjentakende), mentioned in .... ?

$$C_0\sigma_f^2 + k_y^2\left(\frac{1}{2} + \frac{2\tau_i\sqrt{C_0}}{\pi ky}\right)^2 = \frac{4E\gamma_p}{\pi(1-v^2)}$$

Equation 4 Failure criterion cleavage fracture.

C_0 in this case is carbide thickness, τ_i and ky are friction stress and pile-up constant.

The term, $k_y^2\left(\frac{1}{2} + \frac{2\tau_i\sqrt{C_0}}{\pi ky}\right)^2$, has the dislocation input for the cleavage initiation. If it's removed, then as per [18] the equation is reduced "to the Griffith relationship for a grain boundary microcrack." Cleavage fracture sensitivity is affected by a "factor that increases the yield strength, low temperature, triaxial stress state, radiation damage, high strain rate and strain aging" [18]. Not only increases the yield strength with grain size enhancement but also the σ_f increases. For mild steels, smaller grain sizes suggest an elevation in the grain boundary area, this results in smaller grain boundary carbides and an amplification in σ_f. The crucial occurrence usually is the propagation of the microcrack across the first grain boundary it meets. In these cases, as per [18], the Griffith model suggest the following statement for fracture stress [18, s. 238]:

$$\sigma_f = \left(\frac{\pi E\gamma_{gb}}{(1-v^2)d}\right)^{1/2}$$

Equation 5 Griffith model, fracture stress.

Where γ_{gb} is "the plastic work per unit area required to propagate into the adjoining grains" [18]. Because of the "high degree of mismatch between grains in a polycrystalline material $\gamma_{gb} > \gamma_p$" [18].

Sometimes cleavage nucleates, absolute fracture of the specimen or material does not take place [18]. Also," Dolby and Knott derived a modified expression for σ_f based on packet diameter" [18]. In Steel Microstructures and Properties [17] local fracture stress for bainitic and martensitic steels is defined by [17, s. 313]:

$$\sigma_f = \sqrt{\frac{4E\gamma_p}{(1-v^2)d_P}}$$

Equation 6 Fracture stress for bainitic and martensitic steel.

Usually, metal fractures don't break along grain boundaries. Coalescence of voids formed at inclusions and second-phases particles are the most common failure ductile materials. While transgranular cleavage fracture cause brittle fractures. However, some circumstances, can

Kommentert [EH8]: ordlyd ? "påstand ?

make the cracks to propagate along grain boundaries [18]. Intergranular fracture does not have one single mechanism but instead a range of circumstances that can lead to intergranular cracking, including [18]:

1. Precipitation of a brittle phase on the grain boundary.
2. Environmental assisted cracking.
3. Intergranular corrosion.
4. Grain boundary cavitation and cracking at high temperatures.

At grain boundaries brittle phases can be deposited when steel is improper tempered.

Kommentert [EH9]: at = All ?

Kommentert [SR10R9]: done

> "Tempered martensite embrittlement, which results from tempering near 350 C, and temper embrittlement, which occurs when an alloy steel is tempered at ~550 C, both apparently involve the segregation of impurities such as phosphorous and sulfur, to prior austenite grain boundaries" [18].

With steel alloys the breaking can happen at the prior austenite grain boundaries, meaning in between of austenite grains that does not exist. Due to displacive transformations [17].

The separation of aluminum nitride particles at grain borders particles throughout crystallizing is a well-known embrittlement process in cast steel. Also, if present sufficient quantity, it lead to the decreasing of toughness as a result from temper embrittlement in wrought alloys [18].

Environmental cracking can occur in many different material and environment combinations. Crack propagation can be due to corrosion reaction at the crack tip, and the material discriminatingly corrodes at the tip. In other situations, hydrogen embrittlement is the reason for crack propagation. The two cases generate high stresses at the tip and facilitate crack propagation [18].

Relative to their matrix, grain boundaries get weak at high temperatures. A high amount of creep deformation is facilitated by the sliding of grain boundaries. In these cases, void nucleation and grain growth, is mostly found at the tip of the crack. They form as grain boundary cavities grow and coalesce. Grain boundary cavitation is the primary process for the expansion of creep cracks in metals [18].

2.4.3 Environmentally Assisted Cracking

Environmentally assisted cracking, EAC, is a common issue in many industries. The offshore industry, both top side and subsea, have problems with EAC. Subsea its commonly not used higher grade then 8.8 due to Hydrogen Embrittlement. Top side have issues with galvanic corrosion in the splash zone. The term environmentally assisted cracking (EAC) is meant to be generic, as it refers to all cracking in metals that is aided by a chemical environment. There are four recognized types of EAC [18].

1. Stress corrosion cracking (SCC)
2. Hydrogen embrittlement (HE)
3. Corrosion fatigue (CF)
4. Liquid metal embrittlement

Since tempered martensite is very susceptible to, HE, this experiment will focus on this type of EAC. It is well established that very small amount of hydrogen can embrittle strong steel and the hydrogen that embrittles is atomic. As low as 1ppm and hydrogen atoms that are smaller than metallic atoms can fit within interstitial sites in a metallic crystal as well as grain boundaries. Since this hydrogen is diffusible, this phenomenon is also reversible. Should hydrogen be able to diffuse out of the steel then the metal recovers its properties. It's a common opinion that hydrogen decreases the bond strength for the metal atoms by this making fracture easier. Fracture toughness can also be decreased, and subcritical crack growth occurs, both due to the HE. According to [18], Gangloff suggests that cack propagation due to hydrogen embrittlement should be divided into two categories: hydrogen-environment-assisted cracking (HEAC) and internal-hydrogen assisted cracking (IHAC). Main difference between them is the origin from where hydrogen comes from. Both have concentration of hydrogen in the fracture process zone near the crack tip. High stress triaxiality near the crack tip makes the crystal lattice to grow and therefor the hydrogen solubility increases locally. Zones with embrittlement occurs and along with high stresses results in microcracking in the process zone. Eventually microcracks coalesce with the main crack and results in crack extension. As hydrogen absorption and microcracking continue at the local crack tip, the main crack gradually extends over time [17,18].

Microcracking for HEAC happens closer to the crack tip than it does for IHAC, due to the different sources of hydrogen. With HEACH the hydrogen enters the material at the crack tip. Triaxial stress at the tip along with hydrogen trapping results in high concentrations of hydrogen near the tip. When hydrogen is dissolved in the material, it is called IHACH. Materials get hydrogen charged at high temperatures if exposed to H_2 gas or mixtures containing hydrogen, such as H_2S. When cooled down to room temperature, the atomic hydrogen disperses out from the material. This outgassing takes time, especially with thick sections and because of this hydrogen can remain in the martial for a long time. If a hydrogen charged material has a crack under stress, diluted hydrogen will diffuse to the fracture process zone. Concentration of hydrogen in this zone can be many times higher than the bulk concentration [18]. Figure displayed in appendix G.

2.5 Charpy testing

The Charpy test is a common test for measuring impact energy in structural materials [16]. Standardized test specimen with the dimensions: l=55 ±0,6mm, b=10±0,11mm, w= 10±0,

0075mm, that have a V notch is placed in the bottom of the testing apparatus. From a given height and corresponding initial potential energy a pendulum hammer is released. The pendulum strikes the specimen on the opposite side of the notch and fractures the specimen. The difference in potential energy from the pendulum hammer is equivalent to the energy need to fracture the specimen and is described as follows:

$$\Delta E_P = m * g * (h_i - h_f)$$

Equation 7 Potential energy of pendulum

One of the main purposes of the test is to see if the material undergoes a ductile to brittle transition when the temperature decreases and identify the range of which temperature this transition occurs. Measured impact energy absorption is related to the ductile-to-brittle transition through the temperature dependence. Higher temperatures and energy are relatively large, corresponding to a ductile behavior. When temperature is decreasing, impact energy will change quickly over a small temperature window. Below this change impact energy is at a small value and brittle fracture behavior. Appearance of fracture surface gives a good indication of what kind of fracture is occurring and when it changes [16].

Kommentert [EH11]: forklare hva disse tegnene er?

Kommentert [SR12R11]: Nei, det er for simpelt, sensor vet det.

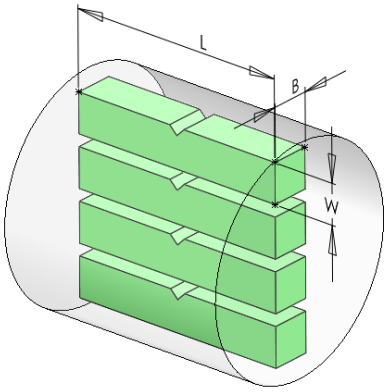

Figure 12 Charpy specimen.

2.6 Tensile testing

When stress is applied most, structures are designed such that only elastic deformation will occur. Should a structure become plastically deformed or experience a permanent change in shape, it may not be possible to function as intended. Tensile test is a stress-strain test and is a commonly used and performed in tension.

> "The test specimen is subjected to an increasing tensile load uniaxially along the axis of the specimen. The tensile testing machine is designed to elongate the specimen at a constant rate, and to continuously and simultaneously measure the instantaneous applied load and the resulting elongations. The test specimen will be permanently deformed and fractured "[17].

The results/raw data is stored as load or force vs elongation. The load-deformation properties depend on the specimen size.

To minimize these geometrical factors, we use engineering stress and engineering strain. Engineering stress σ then has this equation [17, s. 146]:

$$\sigma = \frac{F}{A_0} = MPa$$

Equation 8 Engineering stress.

Where F is the instant load applied perpendicular to the specimen cross section, N, and A_0 is the original cross-sectional area before any load was applied.

The engineering strain is defined with [17, s. 146]:

$$\varepsilon = \frac{l_i - l_0}{l_0} = \frac{\Delta l}{l_0}$$

Equation 9 Engineering strain.

Where "l_i is the instantaneous length and l_0 is original length before any load is applied. This relationship is unitless and normally expressed in percent" [19].

For a brittle and ductile material, the linear part of the ductile curve represents the elastic deformation that the material undergoes. The specimen will revert to its original shape once the applied load is removed. The linear relationship between stress and strain is described by Hooke's Law [16].

The linear section of the ductile curve corresponds to the modulus of elasticity, E-module. The ability to resist elastic deformation is measured with the E-module and brittle material has a higher modulus of elasticity and indicates higher stiffness. Elastic strain resulting from the applied stress is smaller [16].

Point A in Figure 13 represents the yield strength (σ_y) and represents the threshold at which the material can be deformed elastically. Since structures are designed for elastic deformation when exposed to stress, the yield strength is an important mechanical property and is expressed as:

$$\sigma_y = \frac{F}{A_0}$$

Equation 10 Yield strength.

A_0 is the initial cross-sectional area.

Kommentert [EH13]: kilde henvisning?

Kommentert [EH14]: mangler en formel her?

Kommentert [SR15R14]: Nei, fant ut at ikke trenger den. Litt smør på flesk tror eg. Så ser me.

Kommentert [EH16]: korrigere

Kommentert [SR17R16]: done

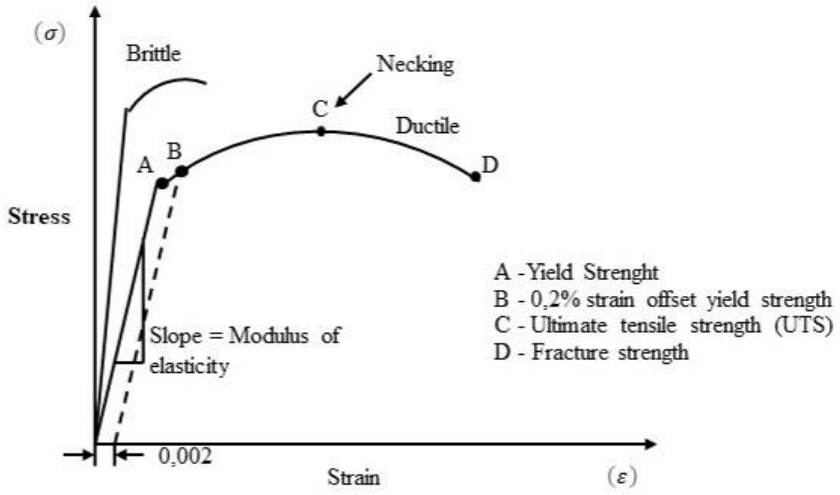

Figure 13 Recreated from [19], Stress-strain curve for a brittle and ductile material.

The transition point from elastic to plastic deformation can be hard to determine for many materials and therefore a convention is established with a linear line drawn parallel to the linear line of the stress-strain curve. This offset is usually 0,2% and is marked as point B in figure 13.

Plastic deformation occurs when the metal is deformed further beyond the yield strength and if the applied force is removed, the material will not go back to its original state. Tensile strength is indicated at point C in figure 13 and is the maximum stress the material in tension is exposed to. Beyond this point, in plastic region, the specimen will undergo all deformation uniformly throughout the measuring region. The necking phenomena will also start at this point and all deformation continuous until fracture. Stress point of facture is at D and is the fracture strength of the material.

For some materials the boundary between elastic and plastic deformation can be hard to determine and therefore a convention

This test was done in compliance with NS-EN ISO 6892-1:2019 [25] and the experiment used cylindrical test pieces with diameter of 10mm.

2.7 Vickers hardness testing

Local resistance against plastic deformation is measured with Vickers hardness test and it's an important mechanical property. A tiny diamond with pyramidal geometry is pushed into the material. The depth and size of the of the indentations are measured by the microscope and converted into Vickers hardness value (HV). The formula for Vickers hardness is [16]:

$$Hv = 1{,}854 * \frac{P}{d_1^2}$$

Equation 11 Vickers hardness.

P is applied load in kg and d_1 is length of the square shaped indentation's diagonal.

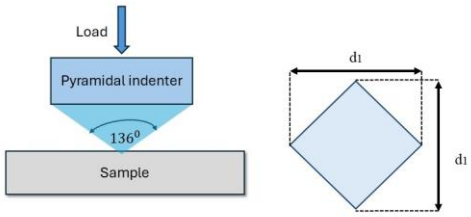

Figure 14 Reproduction from [19]:" Schematic illustration of Vickers hardness test. A pyramidal indenter penetrates the surface of a sample with a given load (left). The diagonals of the resulting indent is measured with the optical".

2.8 SEM / EBSD / EDS

2.8.1 SEM

Scanning electron microscopy (SEM) is a fundamental tool in the arena of material science, it can provide surface images when examined at nano levels. Unlike optical microscopes, SEM uses electrons which have a much shorter wavelength than light and can resolve objects even smaller than several nanometers This capability is absolutely essential when studying

Kommentert [EH18]: eq nr.

Kommentert [SR19R18]: Den har jo det. Problemet er også at figur nr kommer til å forandre seg fremdeles, er bilder lengre oppe som ikke er med.

Kommentert [EH20]: nummerering

Kommentert [SR21R20]: Ka tenke du på her?

nanostructures that are beyond conventional light microscopy's resolution limits. [20].

In fields as diverse as biology, medicine and materials science, SEM is increasingly essential. This is accomplished by detecting secondary electrons, which are ejected from the specimen's surface by the electron beam. The intensity of these electrons varies according to the fact that is tested (topology) of a specimen surface, thus structure detail can be read out in high definition form using SEM. Images can show the surface of a specimen and the fine details that it contains.[20]

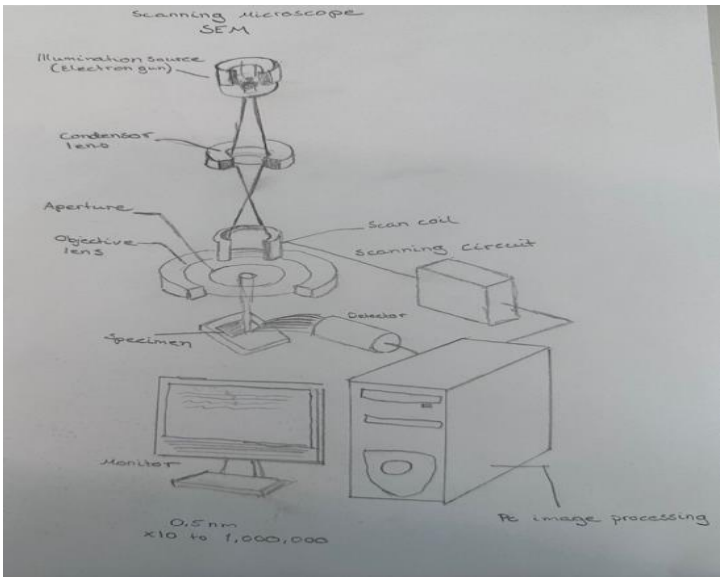

Figure 15 Reproduced from [14], Schematic overview of SEM.

2.8.2 EBSD

SEM not only has the capability of basic observation, but can be also equipped with Electron Back Scatter Diffraction (EBSD). It is able to perform a detailed crystallographic analysis and displays the crystal orientations of materials. In materials science, where polycrystalline materials are predominant, this technique is particularly useful because grain boundaries and

crystal orientations must be understood. EBSD operates by detecting back-scattered electrons that have been diffracted through crystalline samples [20]

2.8.2.1 Parent Austenite grain reconstruction by MTex and EBSD

Kommentert [EH22]: heeeeer mangler noe

Kommentert [SR23R22]: Stemmer det

Mtexis a free Matlab toolbox for analyzing and modeling crystallographic textures by means of EBSD or pole figure data. It's a free and open source basis by an interdisciplinary team of material scientists, geologists and mathematicians [21].

This was used in this thesis to reconstruct the parent austenite phase from a measured martensite phase. The parentGrainReconstructor guesses (Gaussian distribution), based on the EBSD data, what the parent and the child phase is. For an initial guess the Kurdjumov Sachs orientation relationship can be used. Output from this job tells us how much of the parent and child grains and the percentage of already recovered parent grains [21].

Phase transformation from austenite to martensite is not described by a fixed orientation relationship. The actual orientation relationship must be found for each sample individually and for that calcParent2Child function is used. It starts with our initial guess of the OR and repeats against a more suitable OR [21].

With these techniques and commands for removing small grains, misfit for child to child grains and variant graph based parent grain reconstruction. The script prints the possible austenite grain orientation, probability of the best fit for each grain and gives us the mean grain size and standard deviation.

2.8.3 EDS

Another useful attachment to SEM is Energy Dispersive Spectroscopy (EDS), which greatly enhances its analytical capabilities.

The specimen's elemental composition is established by EDS. When an electron beam hits a

sample's surface, X-rays are emitted. These X-rays have energies characteristic of the elements from which they come, allowing high accuracy elemental analysis and mapping to be done. For applications such as verifying material composition, examining impurities and inspecting the distribution of elements in a sample this capability is essential [20].

3 Methodology

3.4 Optical Testing methodology

Samples from the bolts' shanks and heads, which were polished and examined using a SEM (Jeol JSM-IT800), EDS or EBSD, and an optical microscope (Olympus GX53). Figure 16 show the location of specimens in bolt shank.

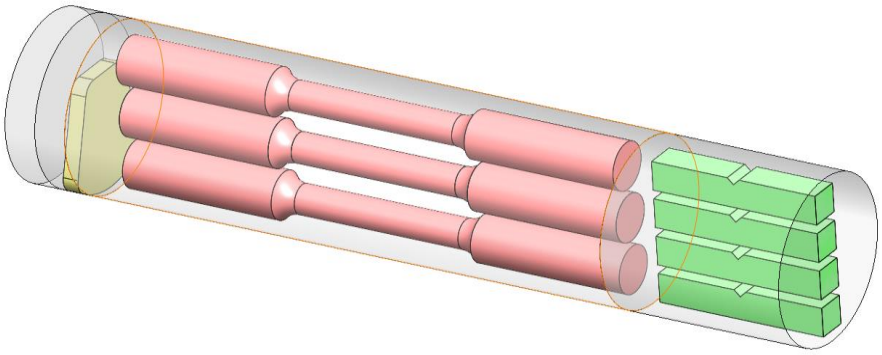

Figure 16 Illustration of samples from bolt shank.

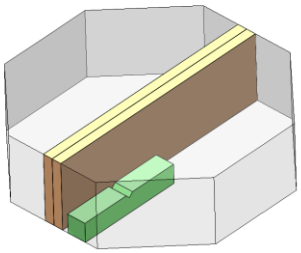

Figure 17 FAH Samples from bolt head.

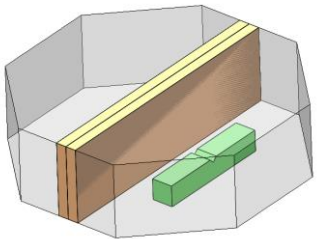

Figure 18 FBH Samples from bolt head.

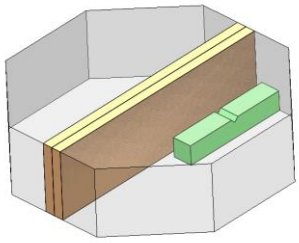

Figure 19 FCH Samples from bolt head.

3.4.1 Specimen Preparation for Optical Testing

Samples was cut using the Struers Discotom 10 to avoid introducing mechanical stresses, After cutting off a section, the piece was cleaned with ethanol solution; then dried on its own for good measure so no debris or outside impurities remained.

Figure 20 Overview of shanks, bolt heads, fracture surfaces and shank specimens.

Two cuts from each head were made to microstructure samples, shown in figure 21,22 &23

Figure 23 FAH Microstructure samples.

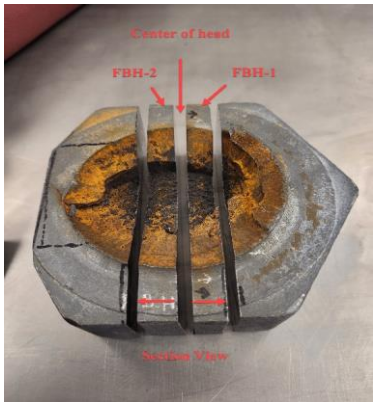

Figure 22 FBH Microstructure samples.

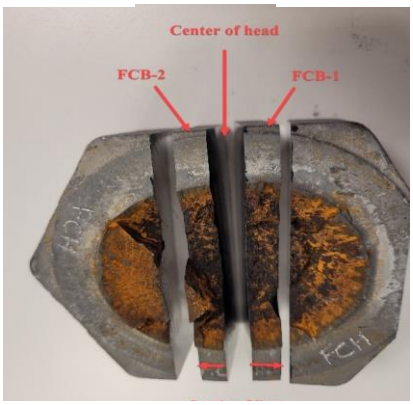

Figure 21 FCH Microstructure samples.

Mounting

Clean samples was hot mounted using the Struers Citopress-30. Bolt heads were mounted in epoxy resin, and bolt shanks in Polyfast resin for its electrical conductivity, suitable for SEM. Mounted samples were grinded and polished with the Struers Tegrapol-35 to achieve smooth, scratch-free surfaces. Given procedures followed, with the final steps repeated three times as there was difficult to remove all scratches from prior steps.

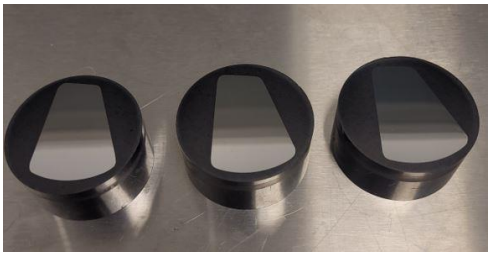

Figure 24 Finished mounted specimens from bolt shanks.

Specimens mounted in a sample holder for consistent treatment.
Shank specimens - washed in the ultrasonic cleaner Struers Lavamin between each steps.
Bolt heads was too large for Lavamin, cleaned with ethanol and blow-dried with air pressure.
Tegrapol-35 was thoroughly cleaned between steps to avoid contamination.

Table 3 Grinding and polishing of shank samples, Program D.

Grinding and polishing of Shank samples, Program D				
Material	Duration, min	Coarseness	Number of cycles	Lubricant
Paper	2	80, grit	1	Water
Paper	2	180, grit	1	Water
Allegro	3	9 µm	1	Diapro 9µm
Dac 3	3	3 µm	1	Diapro Dac 3µm
Chem	2	0,25 µm	1	OP-S

Table 4 Alternative grinding and polishing of shank samples.

Alternative grinding and polishing of shank samples				
Material	Duration, min	Coarseness	Number of cycles	Lubricant
Paper	2	500, grit	1	water
Paper	2	1000, grit	1	water
Paper	2	2000 grit	1	water
mol 3	3	3 µm	1	Diapro Dac 3 µm
Chem	2	0,25 µm	1	OP-S 0,25 µm

3.4.2 Etching for Optical Microscopy

Prior to optical microscopy, the parts dipped in 2% Nital solution for 45 seconds. This etching improved the visibility of areas in the micro-structures, enabling one to observe them under a microscope. Etching of specimen from heads revealed residual stress lines inside the heads as shown in figure 25.

Figure 25 Residual stresses within bolt heads.

3.4.3 SEM and EDS of fracture surface

For the examination of fractures by SEM and ideal elements tests (EDS), the fracture surface from the shank were cut, using a Struers Discotom 10. These samples were etched to remove early corrosion that may have occurred during storage. It was used HNO_3, nitric acid, for the etching, and ultrasonic ethanol wash for three minutes. This insured their surfaces were free of contaminants, which could interfere with both SEM examination and EDS analysis. Before and after picture can be displayed in Appendix F.

3.4.4 EBSD

An additional grinding and polishing procedure were necessary for EBSD examination. The shank specimens were subjected to a refined process to prepare them adequately for high-resolution analysis:

- Mounted in a holder to ensure consistent treatment.
- Washed in the ultrasonic cleaner Struers Lavamin between each step.
- Monitoring ensured that scratch-free surfaces were achieved.
- Tegrapol-35 was cleaned between each step to prevent contamination.
- Resin mounting was removed to fit the specimens into the vacuum chamber of the SEM, as well as to reduce charging.
- The EBSD analysis were performed on a Jeol JSM-IT800 with a UF420 EBSD detector by NORDIF.
- For each scan an area of 300x300 µm and 0,2 µm step size was used.

Due to the similar unit cells of martensite and ferrite the EBSD scan was indexed using a ferritic structure. The three test pieces, FAB, FBB and FCB was put into the SEM and two scans was done. One at the edge of the specimen and the other towards the center of the specimen. Thereafter we got the following data outputs:

FAB-Centre, FAB-Edge, FBB-Centre, FBB-Edge, FCB-Centre, FCB-Edge.

This data information was then used later in the Mtex Parent Austenite Reconstruction.

3.4.5 Re-examination with Optical Microscope

Post-EBSD examination, the shank specimens were revisited using the optical microscope to obtain an overview of the pore distribution initially observed. These specimens were hot mounted again in Struers Citopress-30 with Multifast resin and then ground and polished as per the procedures outlined in the table 5.

Kommentert [EH24]: sette inn denne tabellen

Table 5 Grinding and polishing before pore testing.

Grinding and Polishing before Pore testing				
Material	Duration, min	Coarseness	Number of cycles	Lubricant
Paper	4	120 grit	1	water
Paper	4	220 grit	1	water
Paper	4	320 grit	1	water
Paper	4	500 grit	1	water
Paper	4	1000 grit	1	water
Paper	4	1200 grit	1	water
Paper	4	2000 grit	1	water
Allegro	8	9 µm	1	Diapro 9 µm
Mol	5	3 µm	1	Diapro Dac 3 µm
Nap	10	1 µm	1	Diapro 1 µm
Chem	7	0,25 µm	1	OP-S 0,25 µm

3.5 Mechanical Testing Methodology

3.5.1 Vickers Hardness test

Specimen Preparation for Vickers Hardness Test:

The three specimens from the bolt shank used in the optical tests were prepared for Vickers hardness testing. The preparation involved removing the layer of material that had been etched, following the procedure outlined in table 6 below.

Kommentert [EH25]: oppdatere

Table 6 Polishing for Vickers hardness test.

Polishing before Vickers Hardness				
Material	Duration, min	Coarseness	Number of cycles	Lubricant
mol 3	3	3 µm	1	Diapro Dac 3
Chem	2	0,25 µm	1	OP-S

The aim of this test was to investigate the material's hardness properties as a function of the distance from the outer circumference and across the diagonal of the bolt's cross-section.

Test was executed in accordance with NS-EN ISO 6507-1:2018 [23]. Preliminary tests on the specimens were performed, marked in Figure 26, starting at T1 (2 mm from the outer

circumference) and progressing with 4 mm distance between further impressions to T10 (38 mm from the starting point).

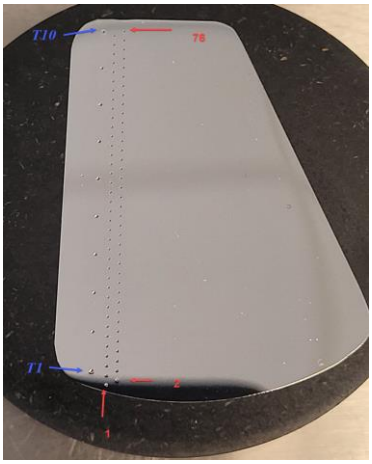

Figure 26 Vickers hardness pattern.

Bolts A, B preliminary test for HV30 10 seconds. Because of complications, bolt C is subject to the same load. The Falcon 5000 hardness testing machine All test was carried out.

The Falcon 5000 was used to measure Vickers hardness values in a series of bolts in both A, B, and C test at HV10 with 10 s dwell time. On figure 26 has marked impress (spaced 0.5mm in X and Y) up to impression 76, at 38mm well over the center of the bolt diameter.

3.5.2 Charpy V-notch test

For each bolt, four test specimens from the shank and one specimen from each bolt head were sectioned for Charpy V-Notch (CVN) tests. Figures 16, 17, 18 and 19 shows the original locations of these test specimens in the bolts.

Kommentert [EH26]: figurer her ?

Kommentert [EH27R26]: unsjuld, det er riktig

The Charpy V-Notch tests were conducted in accordance with NS-EN ISO 148-1:2016.[24] The dimensions for the test specimens are provided in Figure 27. Due to an issue with the

center Charpy specimen from bolt A being cut too short, it was decided to take a specimen from an area closer to the outer circumference for better comparability.

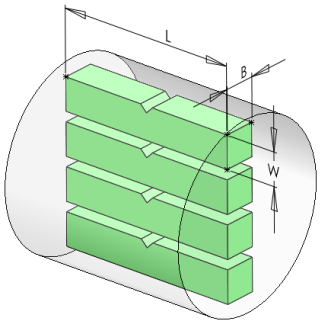

Figure 27 Charpy specimens with dimensions.

The bolts were initially cut using the Struers Discotom 10, an abrasive wet cutting machine with a 2 mm cut-off for each cut. A 55 mm section was cut from each bolt, from which four specimens with a thickness of 10 mm ± 0.06 mm were obtained. Because the specimen areas were too small to be securely mounted, single cutting was employed. The specimens were then adjusted to the desired length and width (l=55 mm ± 0.60 mm, b=10 mm ± 0.11 mm, w=10mm±0,0075mm respectively) using a routing machine, and the V-notch was cut using the Mazak Vertical Smart 430A CNC routing machine.

Tests were conducted on the Zwick/Roell RKP450 machine at room temperature for the shank specimens of appropriate length. The specimens from the bolt heads and shorter shank specimens were tested at -18 degrees Celsius after being cooled in an alcohol bath.

The testing machine was equipped with both digital and analog measurements to record the absorbed energy. Self-centering tongs ensured the proper positioning of the test pieces, and for safety reasons, these were used during testing. After the tests, the absorbed energy was recorded from the digital device, and the fractured surfaces were examined both with the naked eye and using SEM. The fractured samples were stored separately to minimize the risk of damage before SEM examination.

3.5.3 Tensile test

The tensile tests were performed according to NS-EN ISO 6892-1:2019 [25].

Three specimens were prepared for tensile tests. specimens were cut from the bolt using the Struers Discotom 10 to achieve the desired thickness, then shaped into round specimens on a lathe machine. Center holes were created, and the specimens were prepared to be mounted in the Mazak Vertical Smart 430A CNC milling machine to achieve the final dimensions shown in Figure 28.

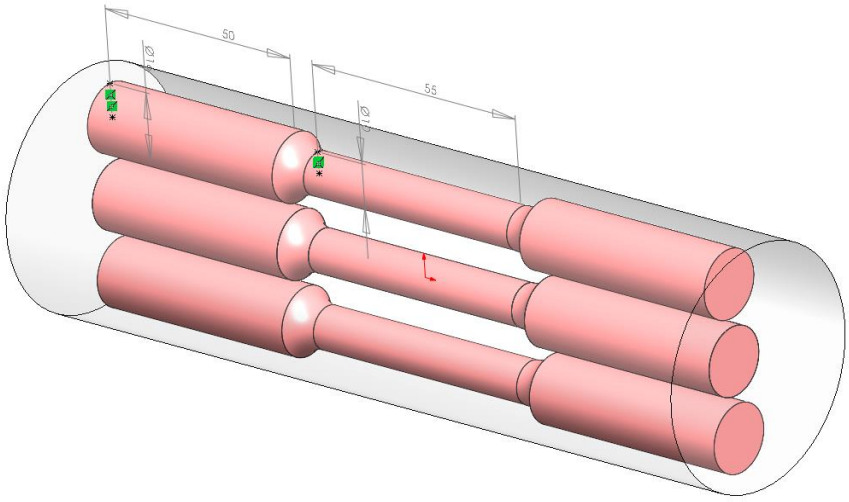

Figure 28 Tensile specimens with dimensions.

The tensile tests were performed on the Instron 5985 testing machine at room temperature. The extensometer had a movement capability of ±10%.

3.6 Parent Austenite grain reconstruction by Mtex and EBSD

For this project it was used a script based on the open source information at the Mtex homepage [21]. Espen Undheim, Senior Engineer, at UiS put together the code that was used and output from the EBSD was used. There was generated pictures of original grainsize and orientation from EBSD scans, reconstructed austenite grains, normal distribution of grain sizes.

4 Results and Discussion

4.1 Macroscopic Examination and Results

A visual inspection shows that the bolt's fracture surface was very different on the bolts. The central area is rough and textured, indicating ductile fracture, while around its edges there was a remarkable contrast between a shiny smooth surface, typical of brittle fractures [16]. This difference practiced between the central part and its periphery must be ascribed to different stress conditions and or microstructural characteristics existing in different parts of bolts [18].

Kommentert [EH28]: figur nr

Figure 30 Fracture surface bolt A.

Figure 29 Fracture surface bolt B

Figure 31 Fracture surface bolt C

The bolt heads were covered in white rust, indicating that they had oxidized and undergone corrosion from contact with humidity. Exposure to moisture and plus saline conditions are probably responsible for this case [3].

Figure 32 White rust on bolt head.

Kommentert [EH29]: figur nr

4.2 Optical microscopy observations

Figure 33 FAH-2 50X possible ductile crack growth.

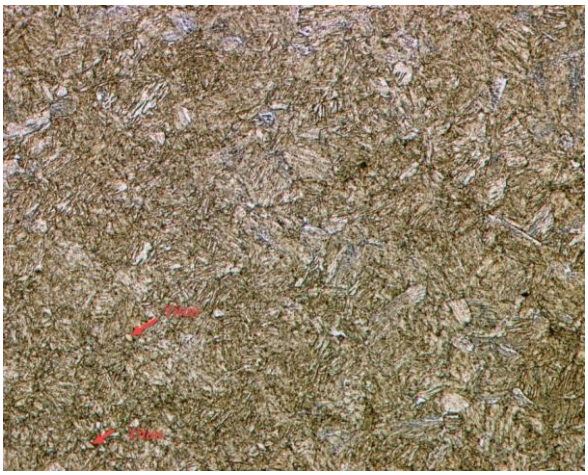

Figure 34 FBH-2 Center, tempered martensite with Titan.

Figure 35 FCH-1 50X possible ductile crack, zig zag pattern.

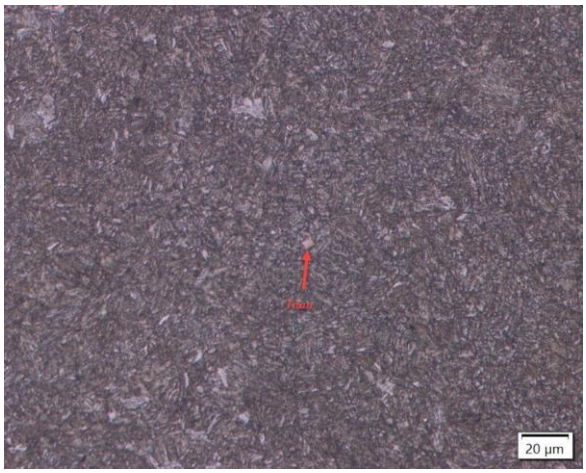

Figure 36 FAB-Shank-26mm from edge, tempered martensite with Titan.

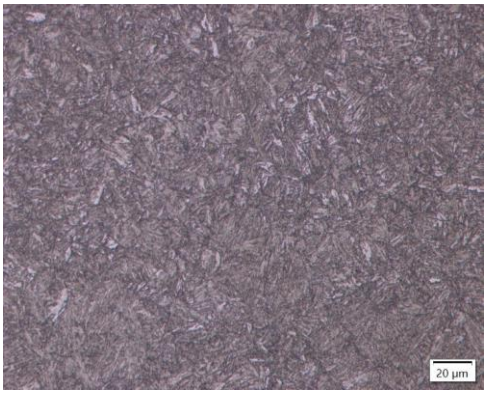

Figure 37 FAB-Shank-Edge, most likely tempered martensite.

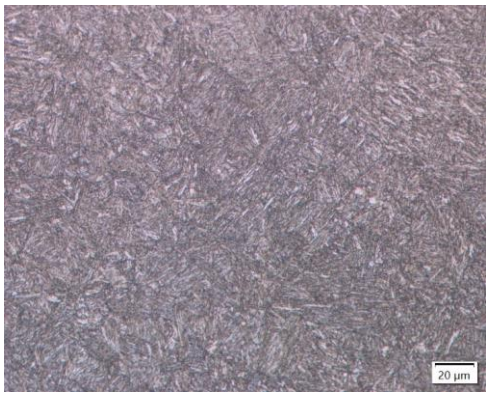

Figure 38 FBB-Shank Edge

As we can see from the pictures taken with the optical microscope all the microstructures seem to be tempered martensite. We can find evidence of Titanium alloy in figure 34 and 36. Signs of fractures typical for possible ductile materials, figure 33 and 35. It has not been easy to extract any more conclusive evidences from the optical microscope observations.

4.3 Optical pore test

The pore analysis of specimens FAB, FBB, and FCB gives insight to porosity characteristics and material quality. All measurements have been done on the same time to ensure equal parameters.

Table 7 Pore analysis FAB.

FAB						
Region (mm)	Number of Pores	Mean Pore Size (µm^2)	Standard Deviation (µm^2)	Minimum Pore Size (µm^2)	Maximum Pore Size (µm^2)	Area Fraction ROI (%)
0-2	1883	5,86	45,06	1,36	1880,00	0,20
6-8	3375	7,67	59,33	1,36	3372,00	0,48
12-14	2871	7,59	53,93	1,36	2868,00	0,42
24-26	3600	7,83	60,34	1,36	3597,00	0,53
34-36	2181	7,96	47,05	1,36	2178,00	0,32

Table 8 Pore analysis FBB.

FBB						
Region (mm)	Number of Pores	Mean Pore Size (µm^2)	Standard Deviation (µm^2)	Minimum Pore Size (µm^2)	Maximum Pore Size (µm^2)	Area Fraction ROI (%)
0-2	4236	7,28	68,10	1,36	4233,00	0,57
6-8	4113	8,18	66,04	1,36	4410,00	0,63
12-14	3558	9,56	69,04	1,36	3555,00	0,65
24-26	3983	7,40	63,75	1,36	3980,00	0,55
34-36	2552	8,80	51,58	1,36	2549,00	0,43

Table 9 Pore analysis FCB

FCB						
Region (mm)	Number of Pores	Mean Pore Size (µm^2)	Standard Deviation (µm^2)	Minimum Pore Size (µm^2)	Maximum Pore Size (µm^2)	Area Fraction ROI (%)
0-2	319	12,50	140,06	1,36	2482,62	0,07
6-8	2218	7,32	47,34	1,36	2215,00	0,29
12-14	1122	7,32	33,95	1,36	1119,00	0,15
24-26	1262	7,56	35,86	1,36	1259,00	0,18
34-36	1690	8,09	41,63	1,36	1687,00	0,26

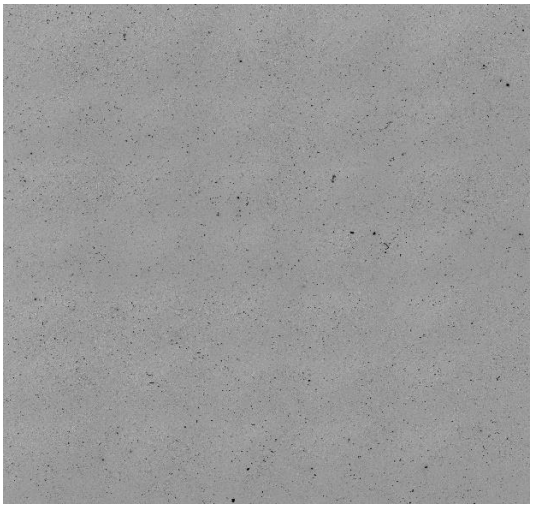

Figure 39 FAB Shank, pores 24-26mm from edge.

FAB and FBB have pore densities remarkably higher than FCB.
The highest is FBB, which ranges from 2552 to 4236 pores: while for FCB, 319 to 1178.
FCB show the largest mean pore sizes, note the 0-2mm region.
FAB instead shows the smallest mean pore sizes.

FAB and FBB has a relatively good consistency of porosity between different locations with some variations across areas. FCB shows more variability in porosity, particularly in the 0-2mm region.
FCB has the most variable pore sizes. Pore size of FAB and FBB varies in the same range

4.4 SEM fracture surface and EDS results

Table 10 EDS results bolt A, with K Line series.

Element	Wt%	Wt% Sigma	Atomic %
Mg	0.01	0.01	0.03
Al	0.07	0.01	0.14
Si	0.26	0.01	0.51
P	0.03	0.01	0.06
S	0.02	0.01	0.03
Ti	0.11	0.01	0.12
Cr	1.45	0.01	1.55
Mn	0.87	0.01	0.88
Fe	97.19	0.03	96.68
Total	100.00		100.00

Table 11 EDS results bolt B, with K Line series.

Element	Wt%	Wt% Sigma	Atomic %
Mg	0.03	0.02	0.06
Al	0.13	0.01	0.28
Si	0.35	0.01	0.68
P	0.04	0.01	0.06
S	0.04	0.01	0.07
Ti	0.15	0.01	0.18
Cr	1.47	0.01	1.57
Mn	0.95	0.02	0.96
Fe	96.85	0.03	96.15
Total	100.00		100.00

Table 12 EDS Results bolt C, with K Line series.

Element	Wt%	Wt% Sigma	Atomic %
Mg	0.05	0.02	0.12
Al	0.10	0.01	0.21
Si	0.33	0.01	0.66
P	0.02	0.01	0.03
S	0.03	0.01	0.05
Ti	0.14	0.01	0.16
Cr	1.49	0.02	1.58
Mn	0.99	0.02	1.00
Fe	96.86	0.04	96.20
Total	100.00		100.00

Table 13 EDS Results vs Mill Test Certificate.

	EDS Result Bolt:				Mill Test Certificate
Element	A	B	C	Mean	Cer.
Mg	0,01	0,03	0,05	0,02	
Al	0,07	0,13	0,10	0,10	0,27
Si	0,26	0,35	0,33	0,31	0,24
P	0,03	0,04	0,02	0,04	0,010
S	0,02	0,04	0,03	0,03	0,007
Ti	0,11	0,15	0,14	0,13	0,0460
Cr	1,45	1,47	1,49	1,47	1,180
Mn	0,87	0,95	0,99	0,91	0,82
Fe	97,19	96,85	96,86	97,02	

The EDS scans of the surface fractures all showing just minor differences and well within what be expected. But when we compare the mean value of elements in EDS against the material certificate [22], there are clearly deviations on some alloys. But this is most likely because of the 0,1% uncertainty with the EDS scan.

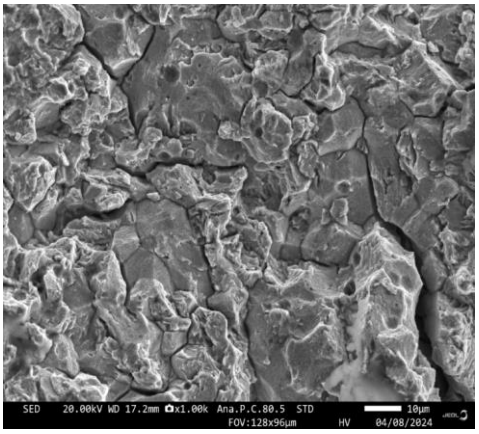

Figure 41 Fracture Surface bolt A near edge, Intergranular cracking.

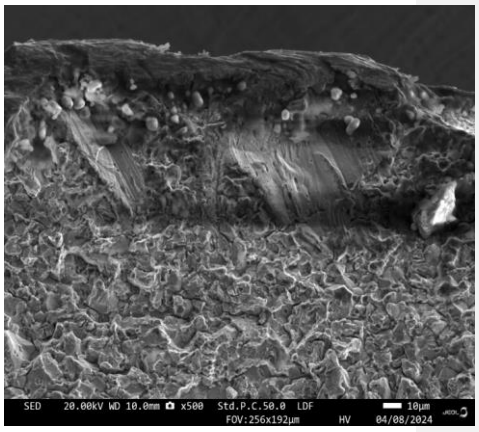

Figure 40 Fracture surface bolt A, at edge, intergranular cracking.

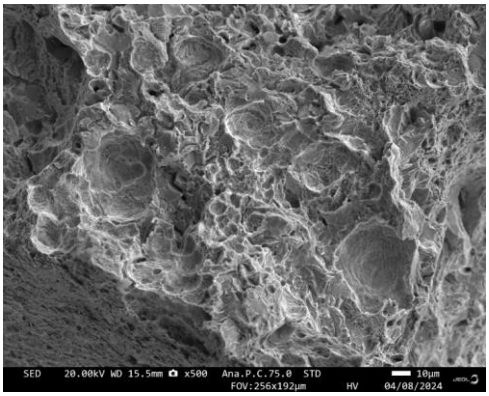

Figure 43 Fracture surface bolt A near center, dimple sections.

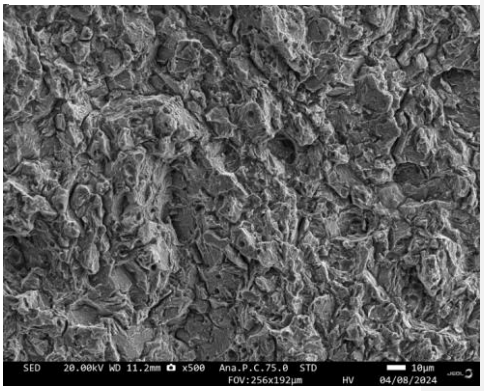

Figure 42 Fracture surface bolt A near center, possible intergranular.

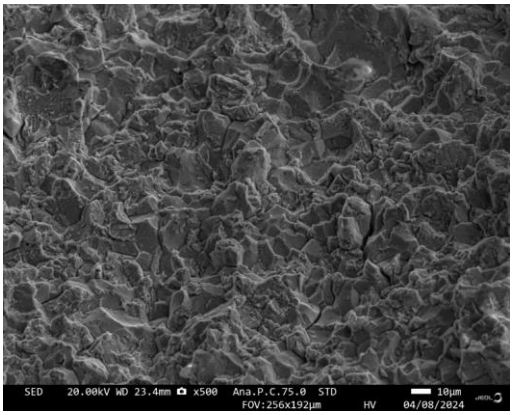

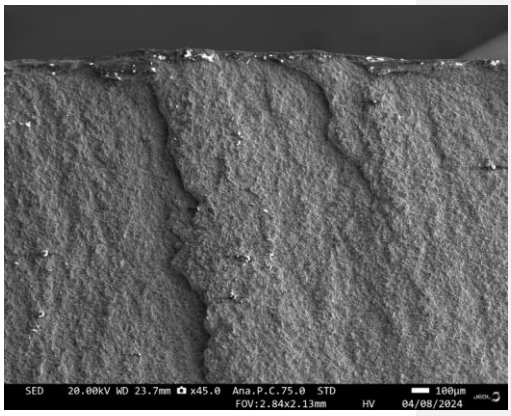

Figure 44 Fracture surface bolt B near edge, brittle intergranular cracking. *Fracture surface bolt B near edge, ratchet marks.*

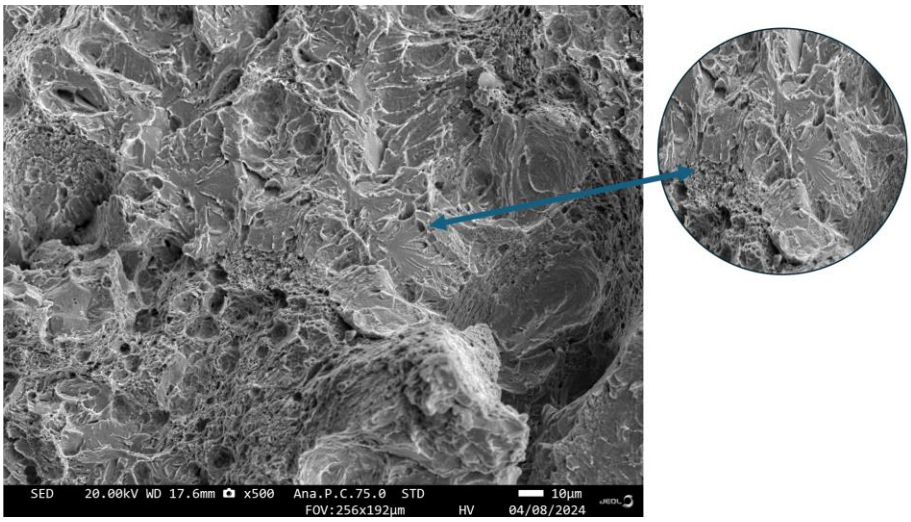

Figure 45 Fracture surface bolt B center, ductile and brittle surface, shown dimples and cleavage fracture.

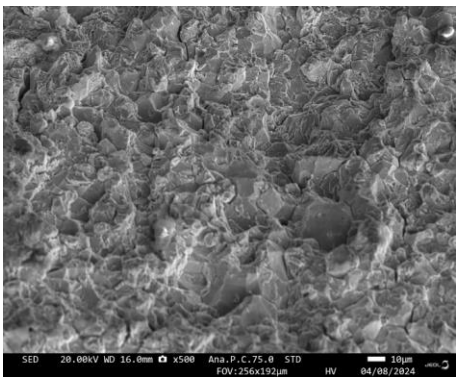

Figure 47 Fracture surface bolt C near edge, intergranular.

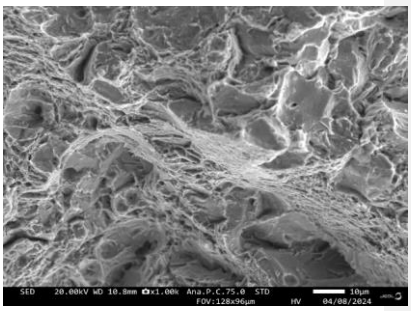

Figure 46 Fracture surface bolt C, near center, ductile.

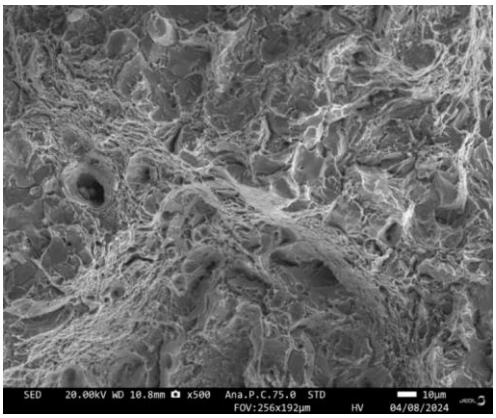

Figure 48 Fracture surface bolt B center, ductile, possible dimples and microvoid.

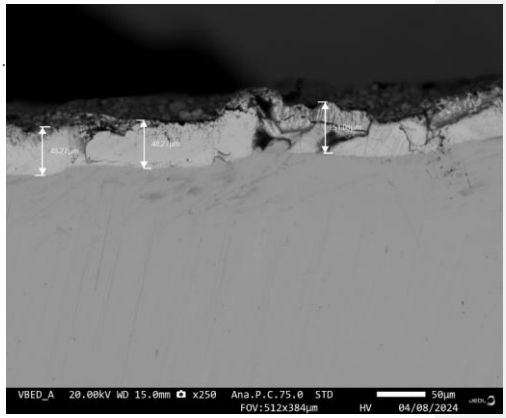

Figure 49 Fracture Surface bolt C, Zn layer.

The pictures shows that all three bolts have signs of intergranular cracking near the edges. Through the transition towards the center of the bolts, they all have possible dimples areas indicating ductile properties. In the center region they have ductile and brittle properties, with dimple at cleavage/intergranular surfaces. Bolt A has the intergranular. The Zn layer was measured at bolt C and was found to be within the requirements given in ISO 10684 [30].

Intergranular fracture several situations that can lead to cracking and one is environmental assisted cracking. There has not been any observation of stress corrosion reaction, SCC, and therefore there is a possibility that the intergranular fracture are due to hydrogen embrittlement, HE.

4.5 Parent Austenite reconstruction by EBDS and Mtex

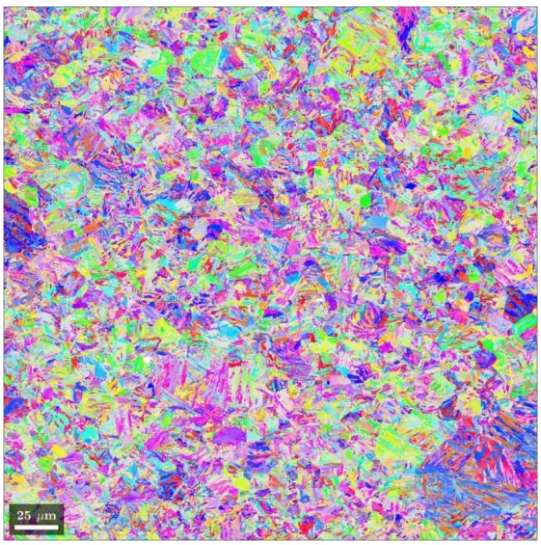

Figure 50 FAB-Edge: Original grain size and orientation from EBSD.

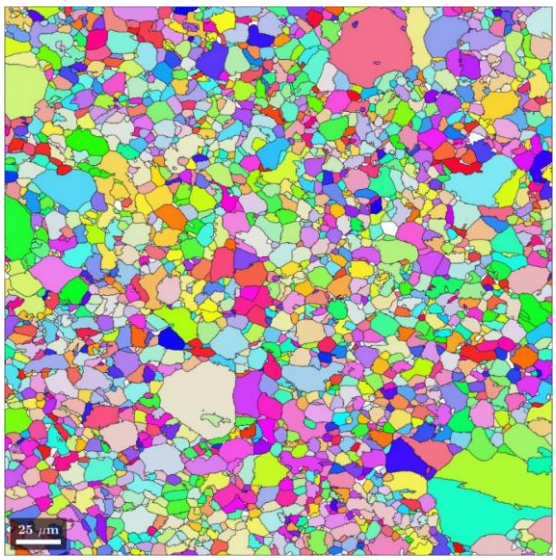

Figure 51 FAB-Edge: Reconstructed Parent Austenite grain size and orientation.

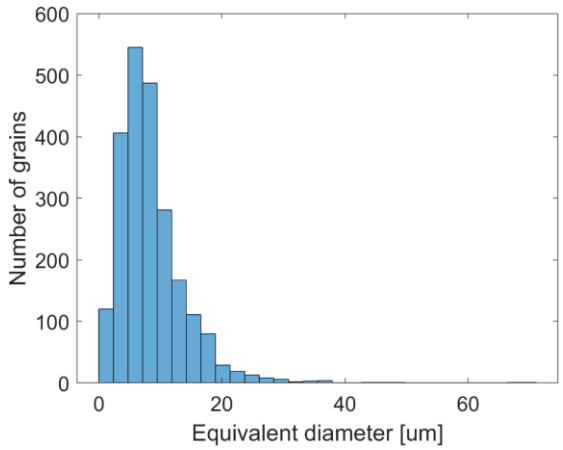

Figure 52 FAB-Edge: Normal distribution of reconstructed parent austenite grain size.

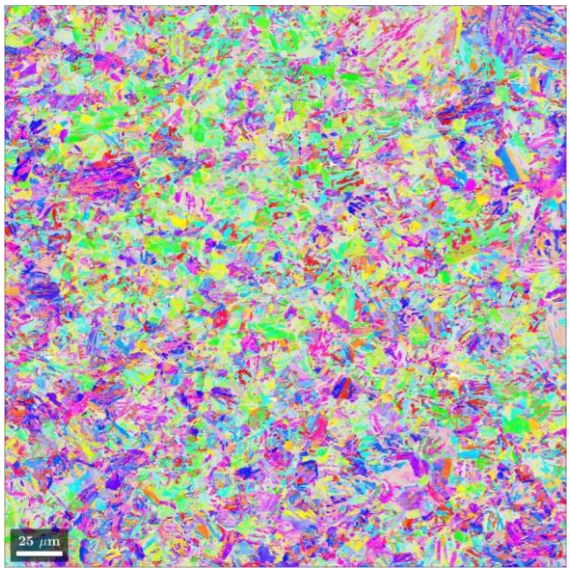

Figure 53 Figure FAB-Center: Original grain size and orientation from EBSD.

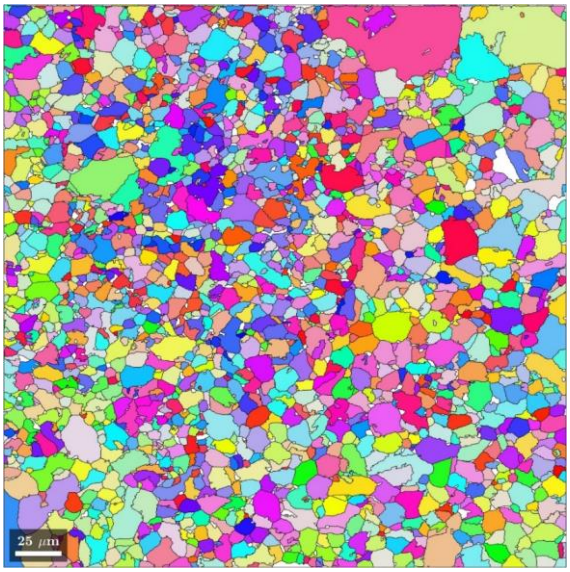

Figure 54 FAB-Center: Reconstructed parent austenite grain size and orientation.

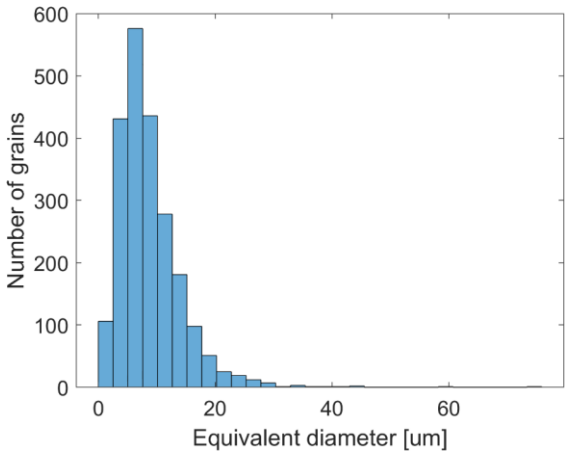

Figure 55 FAB-Center: Normal distribution of reconstructed parent austenite grain size.

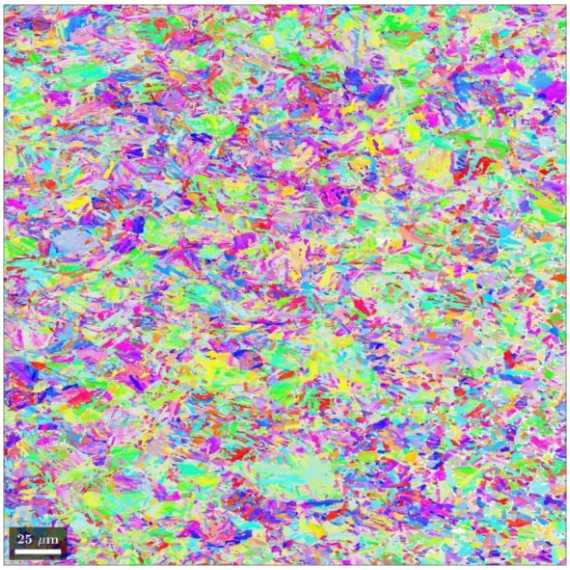

Figure 56 FBB-Edge: Original grain size and orientation from EBDS.

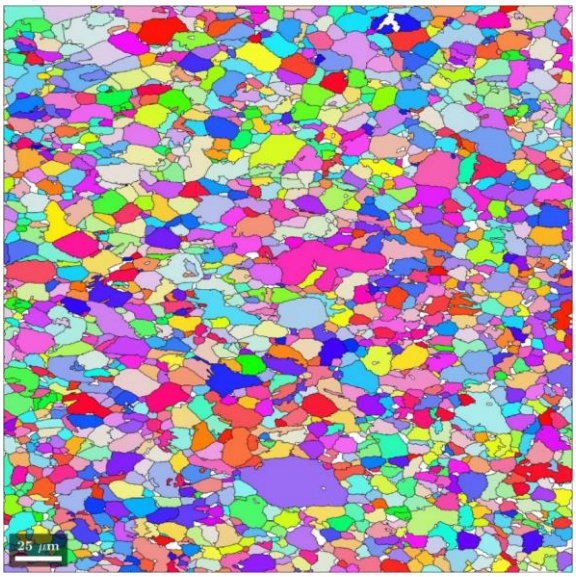

Figure 57 FBB-Edge: Reconstructed austenite grain size and orientation.

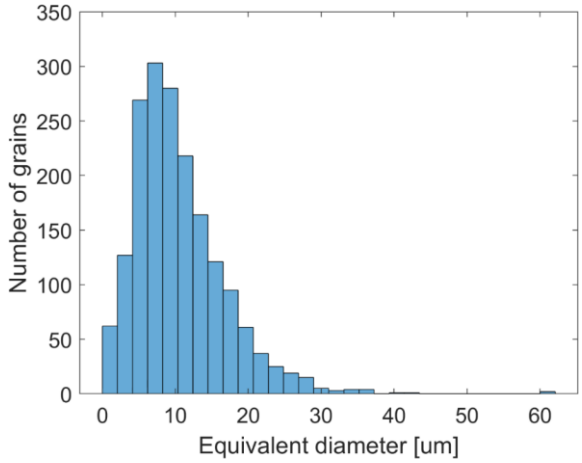

Figure 58 FBB-Edge: Normal distribution of simulated parent austenite grain size.

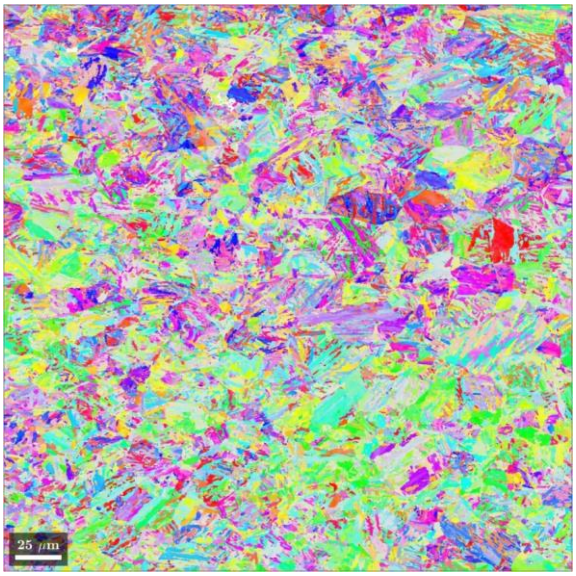

Figure 59 FBB-Center: Original grain size and orientation from EBDS.

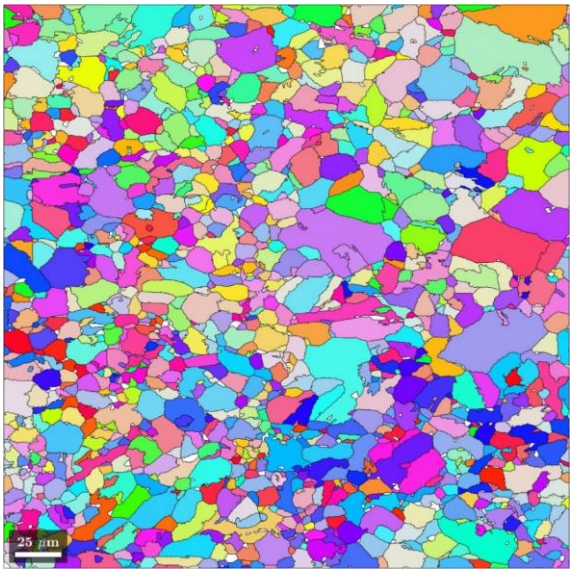

Figure 60 FBB-Center: Reconstructed parent austenite grain size and orientation.

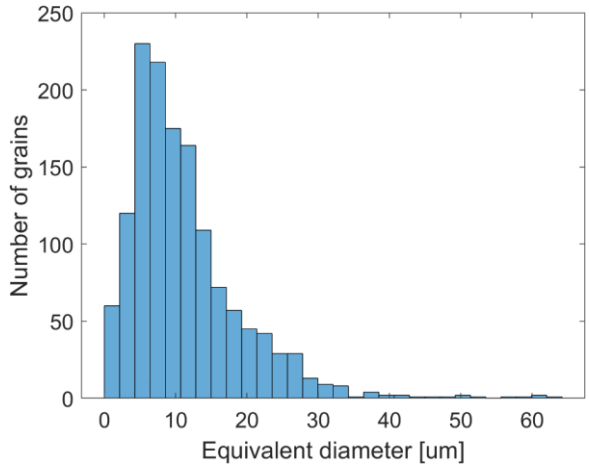

Figure 61 FBB-Center: Normal distribution of reconstructed parent austenite grain size.

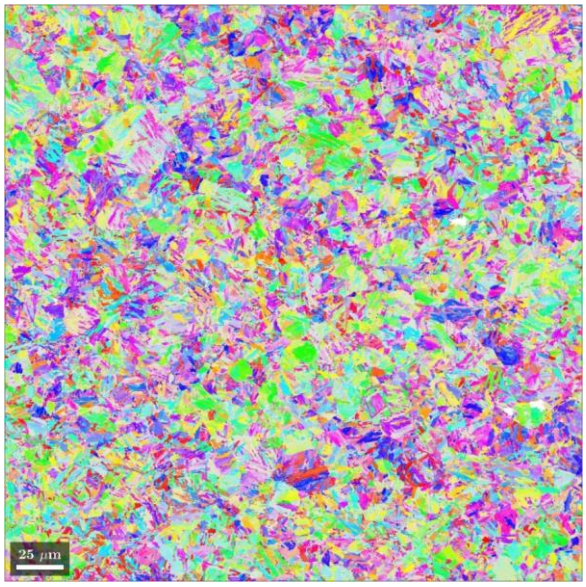

Figure 62 FCB-Edge: Original grain size and orientation from EBSD.

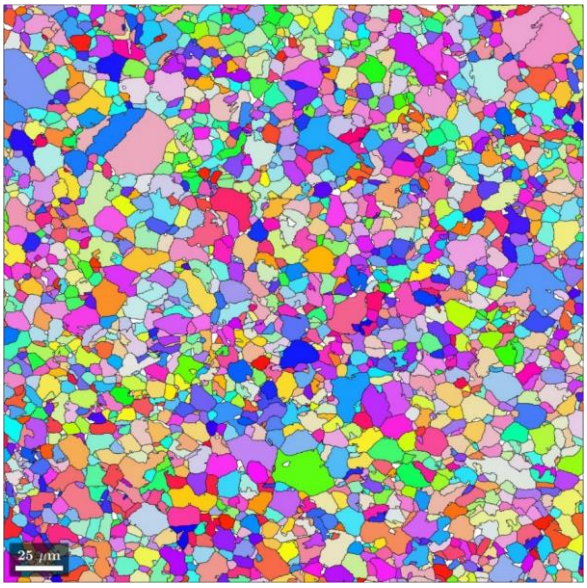

Figure 63 FCB-Edge: Reconstructed parent austenite grain size and orientation.

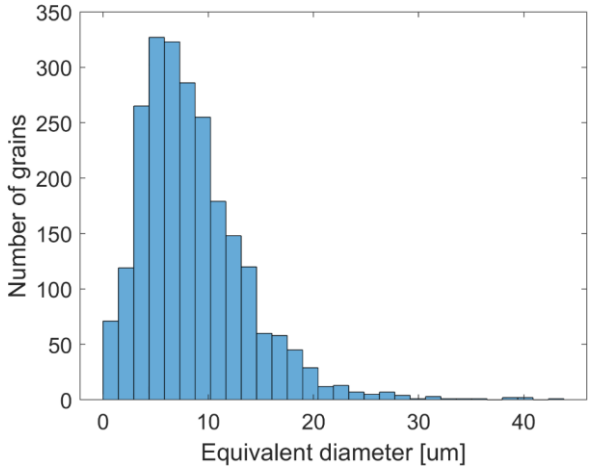

Figure 64 FCB-Edge: Normal distribution of reconstructed parent austenite grain size.

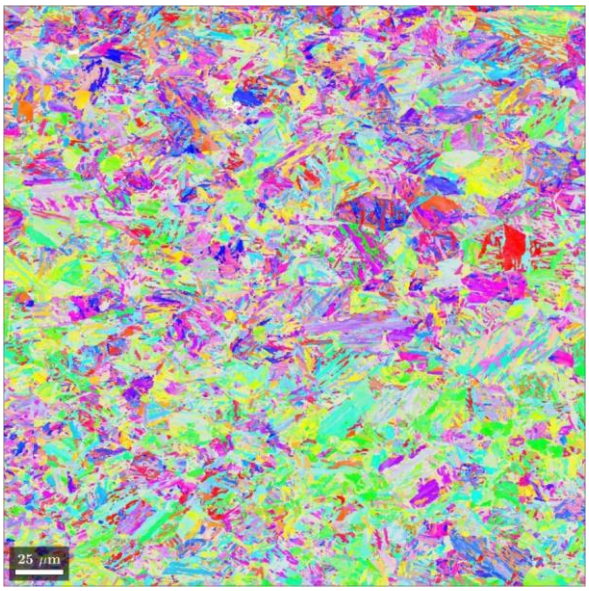

Figure 65 FCB-Center: Original grain size and orientation from EBSD.

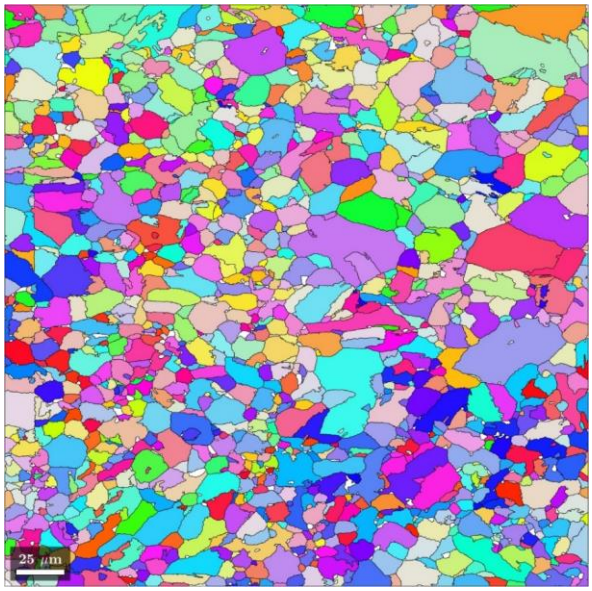

Figure 66 FCB-Center: Reconstructed parent austenite grain size and orientation.

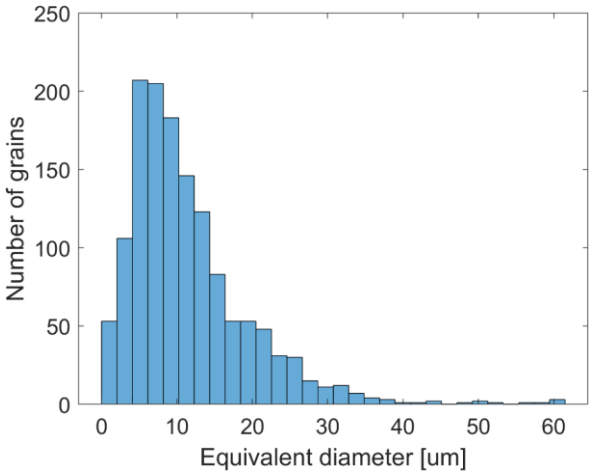

Figure 67 FCB-Center: Normal distribution of reconstructed parent austenite grain size.

Table 14 Mean grain size reconstructed parent austenite.

Specimen	Mean grain size, mm^2	SD	Grain size indices, iso 643
FAB-Edge	0,00383	0,00686	6
FAB-Center	0,00389	0,00686	6
FBB-Edge	0,00474	0,00609	5
FBB-Center	0,00688	0,00993	5
FCB-Edge	0,00373	0,00504	6
FCB-Center	0,00634	0,00984	5

The results of the simulations shows that bolt B and C have smaller grain sizes at edges and A have almost the same. The standard deviations for the results are quite high and this is due to the similarity of the structures for martensite and ferrite. Ferrite has a structure that's only 2-3% stretched with reference to martensite. The smaller grain size should reflect the tensile properties of the specimens, this due to the Hall-Petch relationship [16, s.197]:

$$\sigma_y = \sigma_0 + \frac{k_y}{\sqrt{d}}$$

Where k_y and σ_0 are material constants. All the results are according to NS-EN ISO 643:2020 [14] table B.1 grain size indices 6 or 5.

4.6 Charpy V-notch results

Table 15 Charpy test shank samples.

Charpy Test Shank samples								
NR:	FAB-E	TEMP	FAB-M	TEMP	FBB-M	TEMP	FCB-M	TEMP
1	79,80	room	48,90	-18,00	98,40	room	78,60	room
2	80,20	room	57,20	-18,00	62,90	room	73,80	room
3	83,30	room	40,40	-18,00	70,50	room	67,70	room
4	82,70	room	42,90	-18,00	77,30	room	103,40	room
Mean	81,50		47,35		77,28		80,88	
SD	1,52		6,47		13,22		13,57	

Table 16 Charpy test bolt heads.

Charpy Test Bolt Heads -18C		
	Manuell	Digital
F.A.H	12	12,8
F.B.H	28	28,6
F.C.H	24	23,1

The specimen with max value and the one with min value from each bolt, was then put into the SEM to analyze the fracture surfaces. The specimen was as follows: FAB-M2, FAB-M3, FBB-M1, FBB-M2, FCB-M3 and FCB-M4

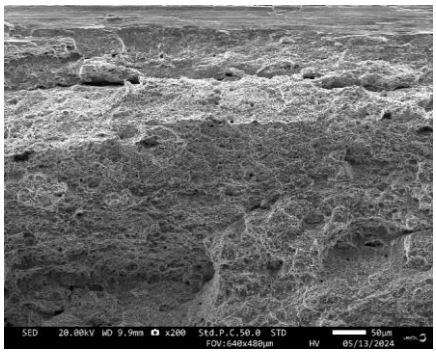

Figure 68 FAB-M2, near fracture surface, ductile, dimples.

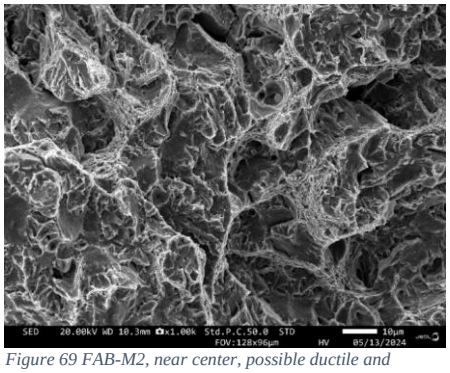

Figure 69 FAB-M2, near center, possible ductile and brittle.

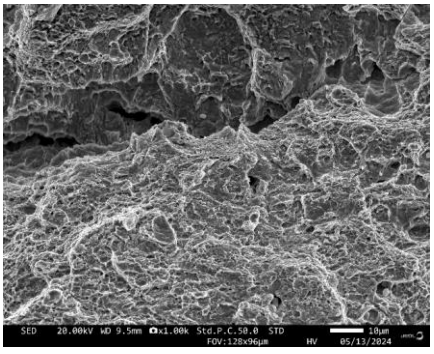

Figure 71 FAB-M3 near fracture surface, ductile, with microvoids.

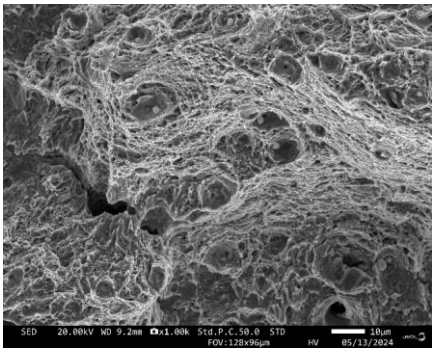

Figure 70 FAB-M3 near center, ductile fracture, possible dimple structure and microvoids.

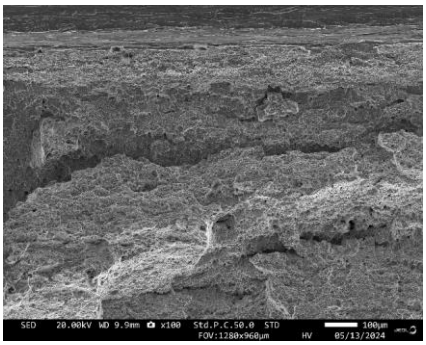

Figure 75 FBB-M1 near fracture surface, ductile, dimple structure.

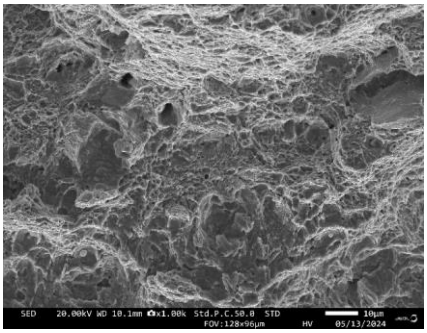

Figure 74 FBB-M1 near center, ductile.

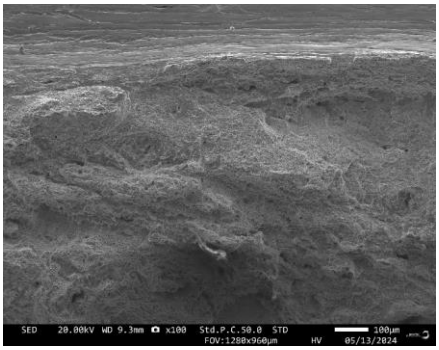

Figure 73 FBB-M2 near fracture surface, ductile, dimple.

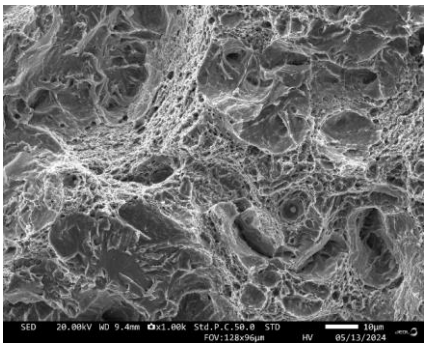

Figure 72 FBB-M2, near center, ductile and brittle, microvoid and cleavage.

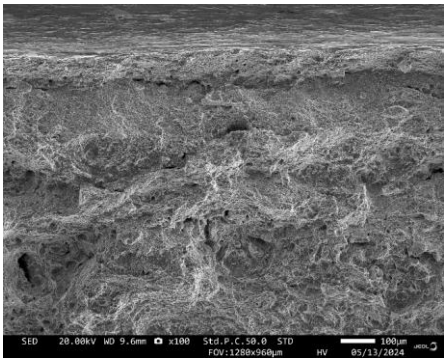

Figure 76 FCB-M3 near fracture surface, ductile.

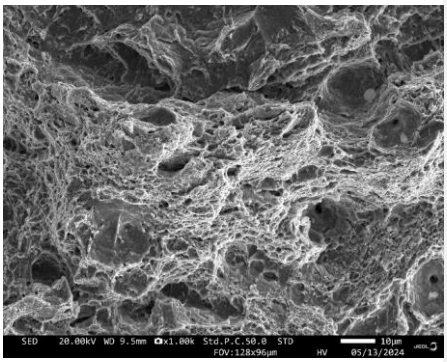

Figure 77 FCB-M3 near center, ductile, dimples.

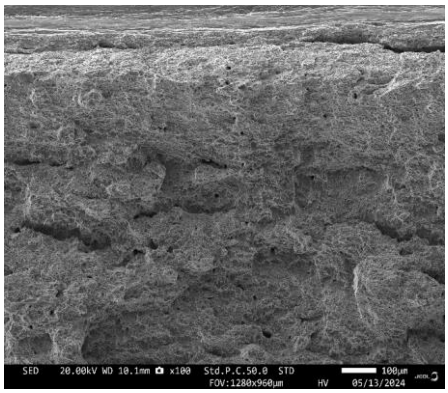

Figure 78 FCB-M4 near fracture surface, ductile.

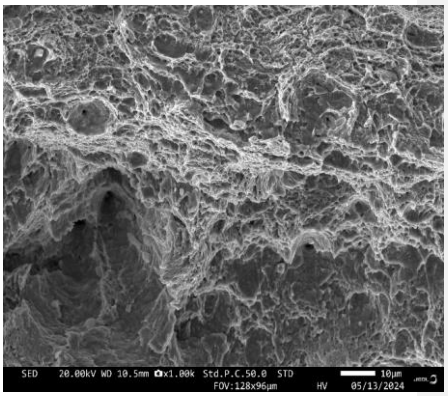

Figure 79 FCB-M4 near center, ductile, dimples.

The SEM pictures from the charpy fracture surfaces showed quite significant differences. At the fracture surfaces from the bolts (FAB, FBB and FCB) they all had intergranular cracks near the edges. This is not in any of the pictures from charpy specimens.

FAB-M2 has ductile surface with nucleated microvoids near the edge. In the center area of the fracture there is possible brittle surface.

FAB—M3 has ductile surfaces both near the edges and center. The center region also has microvoids as sign on ductility.

FBB-M1 has also ductile surface near edge and in the center.

FBB-M2 starts with ductile surface at the edge and transitions to brittle, with cleavage, and ductile dimple surface near the center.

FCB-M3 also is ductile with nucleated microvoids near the edge. This continues into the center area.

FCB-M4 has ductile near the edge and continues to the center.

Generally, all the specimens have mostly ductile surfaces. It was expected to see brittle cracks in FAB-M2 since all those samples had been chilled down to -18 and had the lowest values. But FBB-M2 transitions to a ductile and brittle surface in the center and by that is the sample that is similar to its counterpart at the fracture surface for shank B.

It was unfortunate that the internal positions of the specimens was lost since we would have known what specimen came from the edge and center. Therefor it was not tried to find the transition temperature for each bolt.

4.7 Tensile test

Table 17 Tensile test results.

Specimen	E-Modulus	$R_{P0,2\%}$ [MPa]	Rm [Mpa]	Breaking Strength [Mpa]	Z (%)	A (%)
FAB-M-C	208	1010	1080	726	52,3	13,3
FAB-M-E1	207	1060	1130	710	38,6	12,6
FAB-M-E2	213	1060	1120	689	52,7	14,0
FBB-M-C	209	1020	1090	707	49,1	14,4
FBB-M-E1	200	1070	1130	701	59,2	13,8
FBB-M-E2	199	1050	1120	703	61,6	13,3
FCB-M-C	206	1010	1080	751	41,5	13,1
FCB-M-E1	278	1070	1130	713	61,8	13,1
FCB-M-E2	205	1030	1110	700	60,4	14,1

Yield Strength (RP0.2%) : The yield strengths of the edge specimens are slightly higher than those at center.

Ultimate Tensile Strength (Rm) : Specimens from the outer areas generally reflect this tendency with higher values than center specimens do and much higher than those of center types.

Breaking Strength : The edge specimens also seem to have marginally lower breaking strength than those from center.

Elongation (A%) : Elongation can vary some in the tests, but not to big differences.

The slightly higher results that can be seen in the specimens from the edges can be explained with the smaller grain size we got in the Mtex simulations. They showed that bolts B and also C have smaller mean grain size at the edges. A had the same on edge and center but could be explained with the di tensile indicates smaller. This again can be explained with the bolts being faster cooled down in the outer areas of the bolts then in the center. All the results recorded are within allowed range of the standard.[4]

4.8 Vickers Hardness test

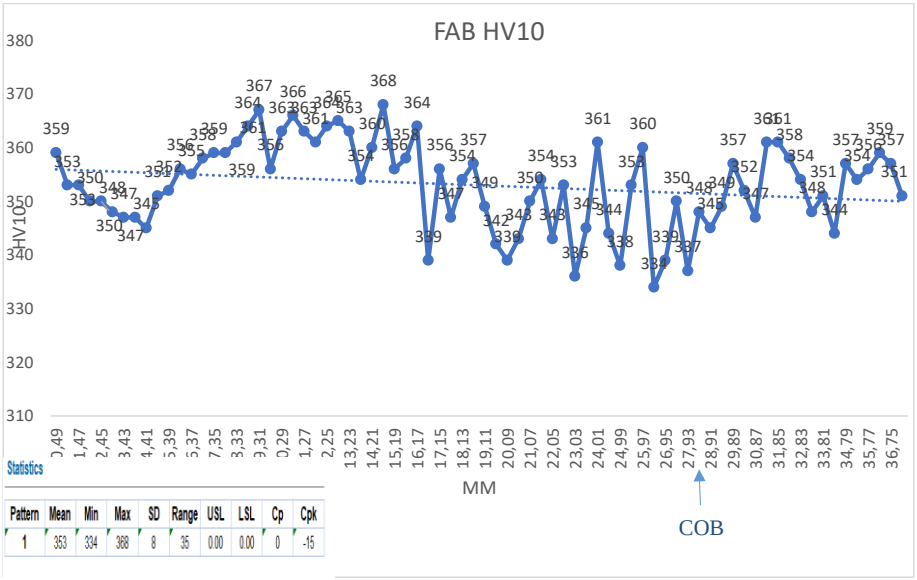

Figure 80 Vickers hardness results FAB.

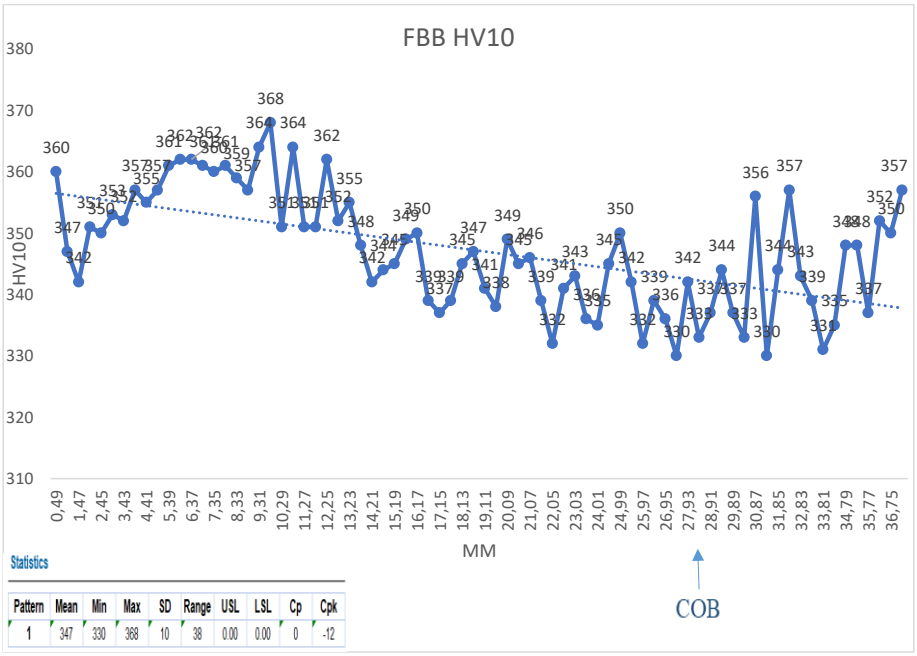

Figure 81 Vickers hardness results FBB.

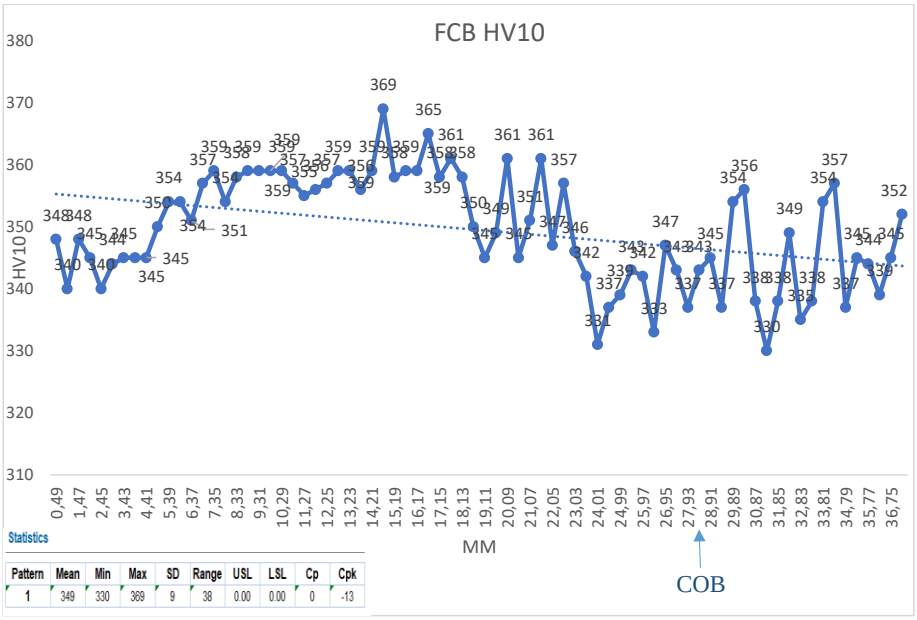

Figure 82 Vickers hardness results FCB

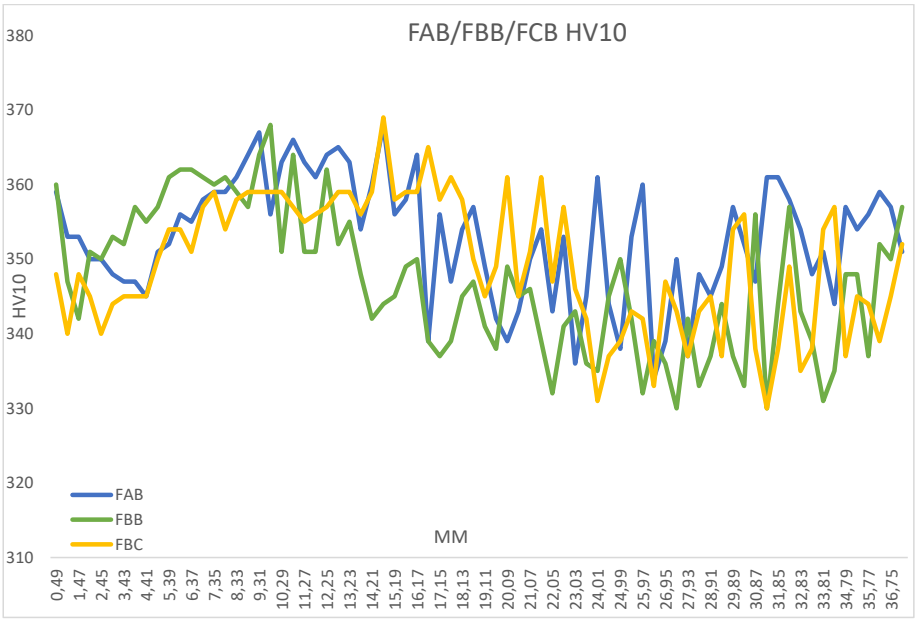

Figure 83 Vickers hardness FAB/FBB/FCB

Table x, y, z represents the results of Vickers hardness test (HV10) for specimens FAB, FBB and FCB. Starting from 0.49 mm on outer edge to 36.75mm passing the bolt center at 28mm.The comparative plot detecting hardness The highest average value is FAB, followed by FCB and FBB. The plot Æ reflects serious differences in hardness level over their length, but when near the middle area it becomes more stable.

4.9 Expert consultation

In this investigation of the bolt failures, participants consulted Angelique Lasseigne, CEO of G2MT Laboratories and a PhD [26]. Answer displayed in Appendix B. But whether hydrogen embrittlement is because of a galvanized coating process, whose move passed through out the subject with electroplating or hot dipped galvanizing, used by that producer, is something to be examined further in accordance with relevant studies [26].

Townsend's [27] study shows that hot-dip galvanizing hydrogen embrittlement retails from

the process consists of a reaction between molten Zn and steel to form a series of intermetallic layers which absorb H2, thus increasing the risk of cracking. Also, defects in the zinc coating at the microscopic level makes it easier for hydrogen to come in, with a resulting serious risk for structural failure [27].

Adding an understanding of hot-dip galvanizing results from both G2MT Laboratories and Townsend's research, underlines the importance of strict galvanizing techniques, and careful handling techniques in general, which can reduce hydrogen pickup and improve the strength and durability of structures.

5 Summary & Conclusion

5.1 Summary

The topic of this thesis is the fracture investigation of M56 high strength bolts (grade 10.9) made from 32CrB4 in on-shore wind turbine towers. Mechanical testing included Charpy Tests, tensile test and Vickers hardness test. Chemical compositions were analyzed by EDS. Microstructural testing's with optical microscope and SEM-EBSD analysis

Bolts generally meet the mechanical requirements. Evidence of intergranular fracture in certain cases, is consistent with hydrogen embrittlement.

None of these findings is enough to set a definite root cause of fracture.

5.2 Concluding Remarks

The tensile tests indicated these particular bolts met standard-required properties, but lack of comparisons with an unfractured bolt would be helpful.

Haven't precisely ruled out hydrogen embrittlement by the hardness tests.

From images of the microstructure, it appears almost all tempered martensite with a few possible ductile cracks grows.

In the SEM images taken, intergranular cracking starts at edge areas and forms a series of strain induced bands which resemble dimples across the center, so both brittle and ductile responses are evident.

Bolt B showed more brittle in character near its core area than the others.

The Charpy samples appeared to be ductile fracture surfaces and there was no intergranular cracking, which suggests that over time the bolts had perhaps leaked out the potential hydrogen.

Hence these results indicate a complex interplay of factors leading to the failures, which require more study to determine their mechanism completely.an unfractured sample.

5.3 Suggestion for future work

The thesis has investigated and explored three fractured bolts by several approaches. Still there are things we would recommend looking further into for further work, that might could set a conclusion for the fractures.

Investigation of similar or unfractured bolts from the same batch. This could give information about external condition of the bolt exterior, but also give results that could be compared to mechanical properties found in this study.

Deep diving into manufacturing procedures to investigate if there is aspects in the production that could cause impurities in the material.

Looking at installation procedures and investigate the knowledge level for the installation personal and requirements allowing individuals to execute the task.

Global finite element methods analysis, taking the entire turbine structure into account. This to check if the forces at the regions where the M56 bolts were used exceeds ULS.

Investigate the material 32CrB4 response to hydrogen and also see if tempering temperature can affect hydrogen embrittlement susceptibility, and thereby decreasing the risk of HE, as has been tested on similar steel, in the article “Effect of hydrogen on mechanical properties and fracture of martensitic carbon steel under quenched and tempered conditions” [28].

6 References

Bibliography

[1] N. Jenkins and J. Ekanayake, “Renewable energy engineering,” Cambridge University Press, Cambridge, 2017.

[2] DNV, "Study on bolt joingt," p. 26, 15 01 2019.

[3] M. B. Lachowicz and M. M. Lachowicz, "Influence of Corrosion on Fatigue of the Fastening Bolts," *MDPI,* p. 17, 15 03 2021.

[4] N. Standard, “NS-EN ISO 898-1:2013,” 2018.

[5] N. Standard, “NS-EN ISO 898-2:2022,” 2022.

[6] Deutsdches Institut fur Normung, “High Strenght hexagon head bolts with large widths across flats for structural steel bolting,” October 1989.

[7] A. Stepanov, A. Koldaev, N. Arutyunyan and A. Zaitsev, "Evolution of the Structural State and Properties of 32CrB4 Steel," *Metals 2022,* p. 366, 12 2022.

[8] Manufacturer, "Mail, Appendix," Oslo, 2024.

[9] "Wikipedia, Hot working," [Online]. Available: https://en.wikipedia.org/wiki/Hot_working#cite_note-Degarmo374-2. [Accessed 25 05 2024].

[10] "Wikipedia Hardening," [Online]. Available: https://en.m.wikipedia.org/wiki/Hardening_(metallurgy). [Accessed 19 05 2024].

[11] *Production of bolts.* [Film]. Norway: Manufacturer, 2016.

[12] Wikipedia, "Wikipedia, Hot-Dip galvanization," [Online]. Available: https://en.wikipedia.org/wiki/Hot-dip_galvanization. [Accessed 13 05 2024].

[13] B. Science, "BoltScience.com," [Online]. Available: https://www.boltscience.com/pages/CommonBoltFailures.htm. [Accessed 19 05 2024].

[14] N. C. C. 4. 1, "NS-EN ISO 643:2020," Norsk Standard, 2020.

[15] G. Y. Long Yang, H. Z. Haoxu Ding and a. B. Y. Shoune Xiao, "method for Evaluating Bolt Competitive," Chinese Journal of Mechanical Engineering, Southwest Jiaotong, 2023.

[16] D. G. R. William D. Callister. JR, Material Science and engineering an introduction, Tenth Edition, 142-171, 181-206, 209-248, Wiley, 2018.

[17] S. H. Bhadeshia and S. R. Honeycombe, Steels Microstructure and Properties, Fourth Edition, Oxford: Butterworth-Heinemann, Elsevier, 2017.

[18] P. T.L Anderson, Fracture Mechanics, Fundamentals and Applications, Third Edition, New York: Taylor & Francis Group, 2005.

[19] F. Tewelde, “Microstructure and mechanical properties of 3D-printed aluminium bronze,” University of Stavanger, Stavanger, 2023.

[20] Jeol, "Jeol.com," [Online]. Available: https://www.jeol.com/products/science/sem.php . [Accessed 18 05 2024].

[21] Mtex, "Mtex," [Online]. Available: https://mtex-toolbox.github.io/.

[22] M. B. Hernandez, “Mill Test Certificate,” Sidenor Aceros Especiales, Spain, 2021.

[23] N. C. C. 4. 1, "NS-EN ISO 6507-1:2023," Norsk Standard, 2023.

[24] N. C. C. 4. 1, "NS-EN ISO 148-1:2016, Metallic materials — Charpy pendulum impact test," Norsk Standard, 2016.

[25] N. C. C. 4. 1, "NS-EN ISO 6892-1:2019, Metallic materials - Tensile testing," Norsk Standard , 2019.

[26] P. Anguelique Lasseigne, *Email, appendix B,* Houston: Anguelique, 2024.

[27] H. Townsend, "Effects of zinc coatings on the stress corrosion cracking and hydrogen embrittlement of low-alloy steel," Metallurgical and Materials Transactions A 6(4):877-883, 1975.

[28] N. D. Adasooriya, W.-s. M. Tucho, E. Holm, T. Årthun, V. Hansen, K. G. Solheim and T. Hemmingsen, “Effect of hydrogen on mechanical properties and fracture of martensitic carbon steel under quenched and tempered conditions.,” *ELSVIER,* p. 11, 2020.

[29] matsusada, "www.matsusada.com," [Online]. Available: https://www.matsusada.com/column/sem-tech2.html. [Accessed 15 05 2024].

[30] N. C. C. 4. 1, "NS-EN ISO 643:2020," Norsk Standard, 2020.

Appendix

Appendix A – Milltest Certificate

sidenor

MILL TEST CERTIFICATE

ISO 9001; IATF 16949; ISO 14001 E ISO 45001

Basauri Plant

SIDENOR ACEROS ESPECIALES S.L.U.
[redacted]
TLF. 944871673 FAX 944871828
www.sidenor.com

[redacted]

Product Made in Spain

CUSTOMER: [redacted]	WORKS REFERENCE: 2168069
REFERENCE: 446570 — SALES ORDER: 339452-1	HEAT NUMBER: 213957
PRODUCT NR: R0553801221 — MASTER REFERENCE: 275606	ROLLED: 18.04.2021

REQUIRED PRODUCT

32CrB4 PLUS ROUND BARS TURNED ANNEALED 55,38-0,12/+0mm ISO h10 6.000/6.200mm NORMAL

EXPEDITION — DELIVERY: 0080731578 WEIGHT (KG): 25.016 BUNDLES: 9 UNITS: 217

MADE ACCORDING TO

DOKKA SP.799.63 C 26.01.2021; EN 10204 - OCT. 2004 3.1; EN 10263-4 - 2017; EN 10278 - 01.10.1999
ISO 898-1 5 2013

CHEMICAL ANALYSIS OF HEAT — U:% HEAT NUMBER: 213957

	C	Mn	Si	P	S	Cr	Ni	Cu	Al	Ti	B
Min.	0,300	0,800	0,100			0,900	0,400				0,0020
Max.	0,350	1,000	0,300	0,015	0,010	1,500	1,100	0,250			0,0035
Cer.	0,330	0,820	0,240	0,010	0,007	1,180	0,790	0,070	0,027	0,0460	0,0032

	H
Min.	
Max.	0,00020
Cer.	0,00012

JOMINY HARDENABILITY — HARDNESS U.:HRC QUENCHING TEMP.:860-5/5ºC

	1,5 mm	3 mm	5 mm	7 mm	9 mm	11 mm	13 mm	15 mm	20 mm	25 mm	30 mm
Min.	50,0	49,0	48,0	47,0	47,0	46,0	45,0	43,0	41,0	39,0	34,0
Max.	56,0	56,0	55,0	55,0	55,0	55,0	55,0	55,0	55,0	54,0	54,0
Cer.	54,0	53,5	53,0	53,0	53,0	53,0	53,0	53,0	53,0	53,0	52,5

JOMINY Standard(EN ISO 642:99 - 01.09.1999)

INCLUSIONS (MICROINCLUSIONS)

Microinclusions std.(DIN 50602 - .09.1985); Type/method(K); K(O):K3 1,4; K(S+O):<= 20

MECHANICAL PROPERTIES OF REFERENCE (CONDITIONS)

Ejec/Suppl/Grade:EN ISO 898-1 10.9
Temperature of:(1):Austenitizing 830ºC; Cooling:(1):Oil
Temperature of:(2):Tempering 520ºC

MECHANICAL PROPERTIES OF REFERENCE (TEST)

Specimen Test location:Tensile:12,5mm from surface; Notch impact: =3 mm; Tensile dir.:Longitudinal
Ts(1.055/1.130MPA):1.082MPa; Ys(Rp(0,2%) >=950MPA):Rp(0,2%) 1.006MPa; El.(5d >=9%):5d 14,9%; Z(>=48%):60,4%
Standard(EN ISO 148-1 - NOV. 2016); N. Impact sample type(CHARPY-V):CHARPY-V
Notch Impact Temp.(-40ºC):-40ºC; K(1):27J; K(2):28J; K(3):28J; K(avg)(>=27J):27,67J; K(single)(>=27J):27J
Surface hardness(320/350HB):342HB; Core hardness(320/350HB):338HB
Hardness at(at 1/2 radius of the bar 320/350HB):at 1/2 radius of the bar 340HB
Specimen Test location:Nucleus; Tensile dir.:Longitudinal
Ts(MPA):1.021MPa; Ys(Rp(0,2%) MPA):Rp(0,2%) 919MPa; El.(5d %):5d 15,6%; Z(%):58,5%

MECHANICAL PROPERTIES AS SUPPLIED (TEST)

Hardness(200/241HB):233HB

ADDITIONAL TESTS (REFERENCE CONDITIONS)

Structure:Tempered martensiteOK

TECHNOLOGY & QUALITY CERTIFIES THAT THE PRODUCT FULL FILLS THE ORDER'S SPECIFICATIONS

APPROVED BY:Miren Begoña Hernandez — SIGN:

DATE:29.06.2021

Page 1 of 2

REF.:1003037370000

sidenor BASAURI

Analyst of Quality certificates

Fig A.1 material certificate.

sidenor

MILL TEST CERTIFICATE

ISO 9001; IATF 16949; ISO 14001 E ISO 45001

Basauri Plant

SIDENOR ACEROS ESPECIALES S.L.U.
Bo. Ugarte S/n. 48970 Basauri (Vizcaya)
TLF. 944871673 FAX 944871828
www.sidenor.com

Product Made in Spain

CUSTOMER:[redacted]		WORKS REFERENCE:**2168069**
REFERENCE:**446570**	SALES ORDER:**339452-1**	HEAT NUMBER:**213957**
PRODUCT NR:**R0553801221**	MASTER REFERENCE:**275606**	ROLLED:**18.04.2021**

ADDITIONAL TESTS (SUPPLY CONDITIONS)

Decarburization:FREE

NON DESTRUCTIVE TESTS

Surface defects std.(EN 10277 - JUNIO 2018); **Surface defects type**(Class 4)
U.T. standard(EN 10308 - 2001); **U.T. type/method**(quality class 4); **ULTRASONIC INSPECTION 100% : O.K.**

ADDITIONAL INFORMATION

Surface and volumetric NDT test are OK

Material melted and manufactured 100% in Spain through the Electric Arc Furnace (EAF) and Vacuum Degassing route (VOD).
Steel not exposed to Mercury, or to any other metal alloy that is liquid, at ambient temperatures during processing or while in Sidenor's possession.
Material dimensionally controlled, visually inspected, and free from radioactivity (<0,1Bq/g concerning a Co-60).
Steel products were not repaired by welding.
100% anti mix test performed.

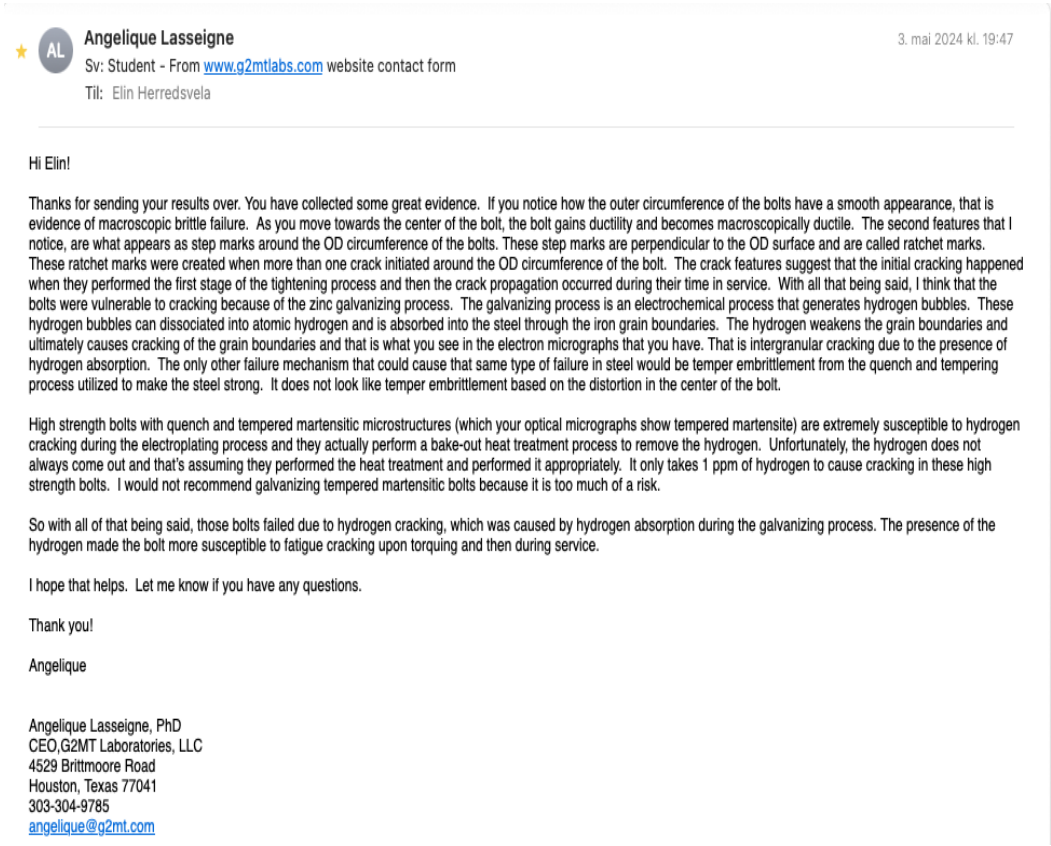

Angelique Lasseigne 3. mai 2024 kl. 19:47

Sv: Student - From www.g2mtlabs.com website contact form

Til: Elin Herredsvela

Hi Elin!

Thanks for sending your results over. You have collected some great evidence. If you notice how the outer circumference of the bolts have a smooth appearance, that is evidence of macroscopic brittle failure. As you move towards the center of the bolt, the bolt gains ductility and becomes macroscopically ductile. The second features that I notice, are what appears as step marks around the OD circumference of the bolts. These step marks are perpendicular to the OD surface and are called ratchet marks. These ratchet marks were created when more than one crack initiated around the OD circumference of the bolt. The crack features suggest that the initial cracking happened when they performed the first stage of the tightening process and then the crack propagation occurred during their time in service. With all that being said, I think that the bolts were vulnerable to cracking because of the zinc galvanizing process. The galvanizing process is an electrochemical process that generates hydrogen bubbles. These hydrogen bubbles can dissociated into atomic hydrogen and is absorbed into the steel through the iron grain boundaries. The hydrogen weakens the grain boundaries and ultimately causes cracking of the grain boundaries and that is what you see in the electron micrographs that you have. That is intergranular cracking due to the presence of hydrogen absorption. The only other failure mechanism that could cause that same type of failure in steel would be temper embrittlement from the quench and tempering process utilized to make the steel strong. It does not look like temper embrittlement based on the distortion in the center of the bolt.

High strength bolts with quench and tempered martensitic microstructures (which your optical micrographs show tempered martensite) are extremely susceptible to hydrogen cracking during the electroplating process and they actually perform a bake-out heat treatment process to remove the hydrogen. Unfortunately, the hydrogen does not always come out and that's assuming they performed the heat treatment and performed it appropriately. It only takes 1 ppm of hydrogen to cause cracking in these high strength bolts. I would not recommend galvanizing tempered martensitic bolts because it is too much of a risk.

So with all of that being said, those bolts failed due to hydrogen cracking, which was caused by hydrogen absorption during the galvanizing process. The presence of the hydrogen made the bolt more susceptible to fatigue cracking upon torquing and then during service.

I hope that helps. Let me know if you have any questions.

Thank you!

Angelique

Angelique Lasseigne, PhD
CEO,G2MT Laboratories, LLC
4529 Brittmoore Road
Houston, Texas 77041
303-304-9785
angelique@g2mt.com

Fig B.1 Email with Angelique

Fig B.2 Email with Angelique

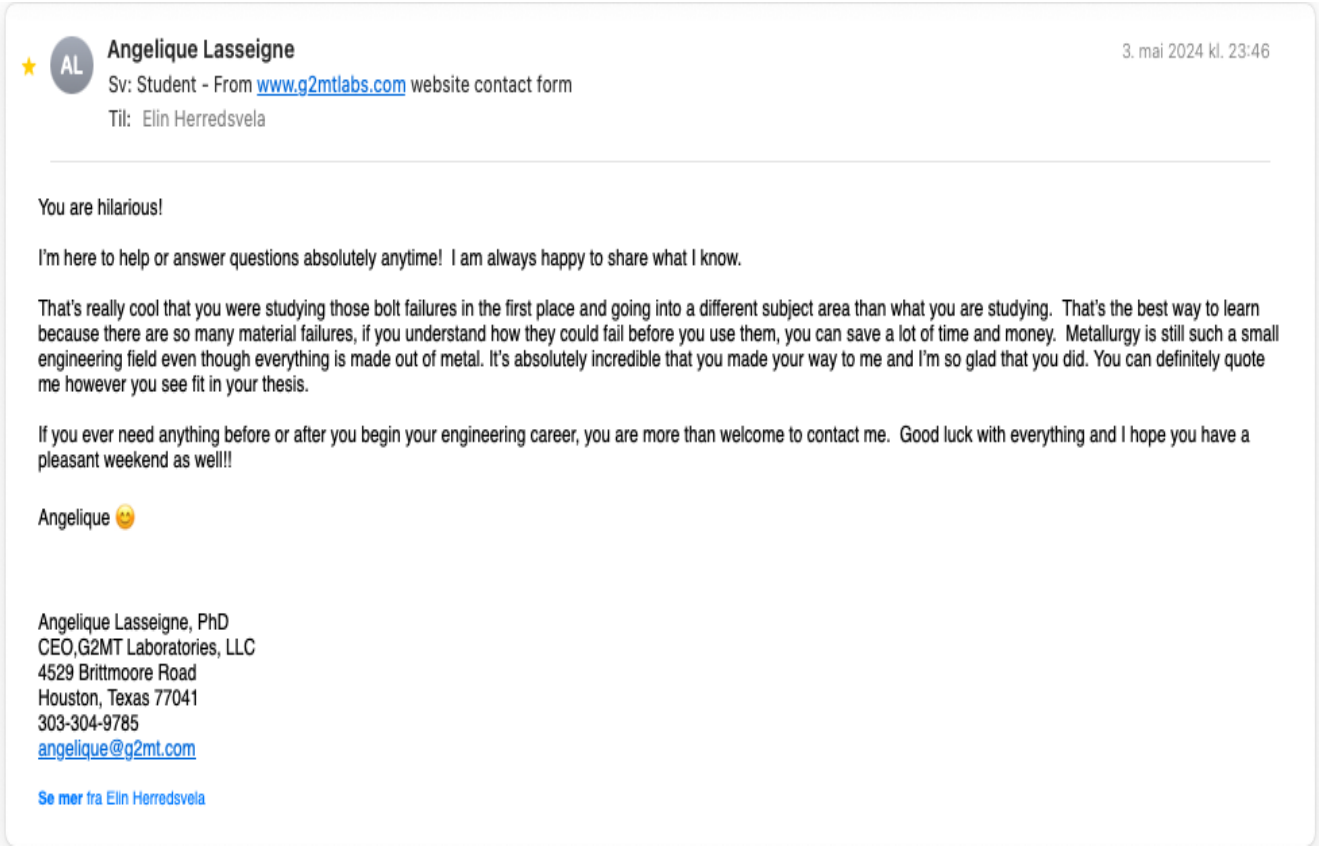

Angelique Lasseigne 3. mai 2024 kl. 23:46

Sv: Student - From www.g2mtlabs.com website contact form

Til: Elin Herredsvela

You are hilarious!

I'm here to help or answer questions absolutely anytime! I am always happy to share what I know.

That's really cool that you were studying those bolt failures in the first place and going into a different subject area than what you are studying. That's the best way to learn because there are so many material failures, if you understand how they could fail before you use them, you can save a lot of time and money. Metallurgy is still such a small engineering field even though everything is made out of metal. It's absolutely incredible that you made your way to me and I'm so glad that you did. You can definitely quote me however you see fit in your thesis.

If you ever need anything before or after you begin your engineering career, you are more than welcome to contact me. Good luck with everything and I hope you have a pleasant weekend as well!!

Angelique

Angelique Lasseigne, PhD
CEO,G2MT Laboratories, LLC
4529 Brittmoore Road
Houston, Texas 77041
303-304-9785
angelique@g2mt.com

Se mer fra Elin Herredsvela

Appendix C – Mail from bolt manufacturer

[redacted]

RE: Bachelor oppgave - Bolt brudd

6. mai 2024 kl. 11:03

Til: Elin Herredsvela, Kopi: Elin Versland Herredsvela, Stig Roar Lyse Rødne

Detaljer

Hei.

Ja, beklager.
Jeg har forsøkt å få en tilbakemelding fra teknisk og kvalitet, men de har ikke kommet med noen feedback.

Jeg kan i hvert fall fortelle dere at vi ikke syrevasker boltene våre, men renser de ved sandblåsing, noe som ikke tilfører hydrogen.
Vi har også et makskrav for hydrogen i stålet vårt.

Det kan hende jeg har misforstått dere, men hva mener dere med elektrogalvanisering?
Dette er varmforsinkede bolter(tZN/HDG/fzv), altså ikke el zink.

Siden boltene har vært montert så kan jeg ikke si noe om hvor hydrogenet ble tilført, det kan ha skjedd før, under eller etter montering.

Produksjonsrekkefølge(oppsummert):

Smi(varmsmidd)
Herding
Herdekontroll
Varmforsinking
Kontroll
Pakking
Lager

Det er en stund siden jeg så over denne saken, så jeg kan ha husket feil.

[redacted]

Internal Sales

[redacted]

[redacted]fasteners.com

FOLLOW US
LINKEDIN | WEB

#STRONGCONNECTIONS

Se mer fra Elin Herredsvela

Fig C.1 Email with bolt manufacturer.

Appendix D – Mtex Script

```
ebsd = EBSD.load('C:\Users\2927409\OneDrive - Universitetet i
Stavanger\Documents - Electron microscopes\EBSD\Stig Roar og
Elin\FCB - Utside -
200_cleaned.h5','convertSpatial2EulerReferenceFrame', 'setting 2')
plotx2east

%rot = rotation.byAxisAngle(xvector,180*degree);
%ebsd = rotate(ebsd,rot,'keepEuler');

% grain reconstruction
[grains,ebsd.grainId] = calcGrains(ebsd('indexed'),
'angle',2*degree);

% remove small grains
ebsd(grains(grains.grainSize < 5)) = [];

% reidentify grains with small grains removed:
[grains,ebsd.grainId] =
calcGrains(ebsd('indexed'),'angle',2*degree);
grains = smooth(grains,5);

% plot the data and the grain boundaries
plot(ebsd('Ferrite'),ebsd('Ferrite').orientations,'figSize','large')
fig = gcf
exportgraphics(fig,'Projects\Test\Original_IPF.png','Resolution',300
)

% set up the job
job = parentGrainReconstructor(ebsd,grains);

job.csParent = crystalSymmetry('mineral', 'Austenite','SpaceID',
225)

% initial guess for the parent to child orientation relationship
%job.p2c = orientation.KurdjumovSachs(job.csParent, job.csChild)
%job.p2c = orientation.GreningerTrojano(job.csParent,job.csChild)
job.p2c = orientation.NishiyamaWassermann(job.csParent, job.csChild)

close all
histogram(job.calcGBFit./degree,'BinMethod','sqrt')
xlabel('disorientation angle')

job.calcParent2Child

hold on
histogram(job.calcGBFit./degree,'BinMethod','sqrt')
```

```
hold off

% compute the misfit for all child to child grain neighbours
[fit,c2cPairs] = job.calcGBFit;

% select grain boundary segments by grain ids
[gB,pairId] = job.grains.boundary.selectByGrainId(c2cPairs);

% plot the child phase
plot(ebsd('Ferrite'),ebsd('Ferrite').orientations,'figSize','large',
'faceAlpha',0.5)

% and on top of it the boundaries colorized by the misfit
hold on;
% scale fit between 0 and 1 - required for edgeAlpha
plot(gB, 'edgeAlpha', (fit(pairId) ./ degree - 2.5)./2
,'linewidth',2);
hold off

fig = gcf
exportgraphics(fig,'Projects\Test\Original_IPF_with_PAG_overlay.png'
,'Resolution',300)

job.calcVariantGraph('threshold',2.5*degree,'tolerance',2.5*degree)
job.calcVariantGraph('threshold',2.5*degree,'tolerance',2.5*degree,'
mergeSimilar')
job.clusterVariantGraph
job.calcVariantGraph('threshold',2.5*degree,'tolerance',2.5*degree)
job.clusterVariantGraph('includeSimilar')

plot(job.grains,job.votes.prob(:,1))
mtexColorbar

fig = gcf
exportgraphics(fig,'Projects\Test\voting_probability.png','Resolutio
n',300)

job.calcParentFromVote('minProb',0.5)
% plot the result
plot(job.parentGrains,job.parentGrains.meanOrientation)

fig = gcf
exportgraphics(fig,'Projects\Test\Original_GB_with_reconstructed_Aus
tenite_minprop_5.png','Resolution',300)

job.calcGBVotes('p2c','reconsiderAll')

% assign parent orientations according to the votes
job.calcParentFromVote

% plot the result
```

```
plot(job.parentGrains,job.parentGrains.meanOrientation)
fig = gcf
exportgraphics(fig,'Projects\Test\IPF_reconstructed_austenite_mean_o
rientation.png','Resolution',300)

% merge grains with similar orientation
job.mergeSimilar('threshold',7.5*degree);

% plot the result
plot(job.parentGrains,job.parentGrains.meanOrientation)
fig = gcf
exportgraphics(fig,'Projects\Test\IPF_reconstructed_austenite_mean_o
rientation_merged_similar.png','Resolution',300)

job.mergeInclusions('maxSize',50);

% plot the result
plot(job.parentGrains,job.parentGrains.meanOrientation)
fig = gcf
exportgraphics(fig,'Projects\Test\IPF_reconstructed_austenite_mean_o
rientation_merged_similar_no_inclusions.png','Resolution',300)

figure(2);

GS_parent = job.parentGrains
pd = fitdist(GS_parent.area, 'Normal')

histogram(GS_parent, 100)
xlabel('Grain area [um^2]')
ylabel('Relative area [%]')



fig = gcf
exportgraphics(fig,'Projects\Test\PAG_Grain_size.png','Resolution',3
00)
```

Appendix E – Tensile tests

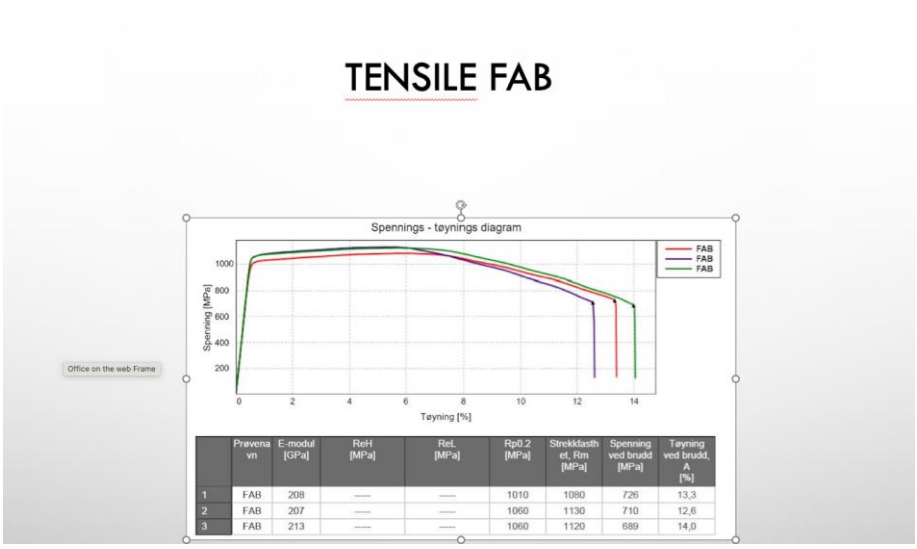

	Prøvena vn	E-modul [GPa]	ReH [MPa]	ReL [MPa]	Rp0.2 [MPa]	Strekkfasth et, Rm [MPa]	Spenning ved brudd [MPa]	Tøyning ved brudd, A [%]
1	FAB	208	-----	-----	1010	1080	726	13,3
2	FAB	207	-----	-----	1060	1130	710	12,6
3	FAB	213	-----	-----	1060	1120	689	14,0

Fig E.1 Tensile result FAB

Office on the web Frame

TENSILE FBB

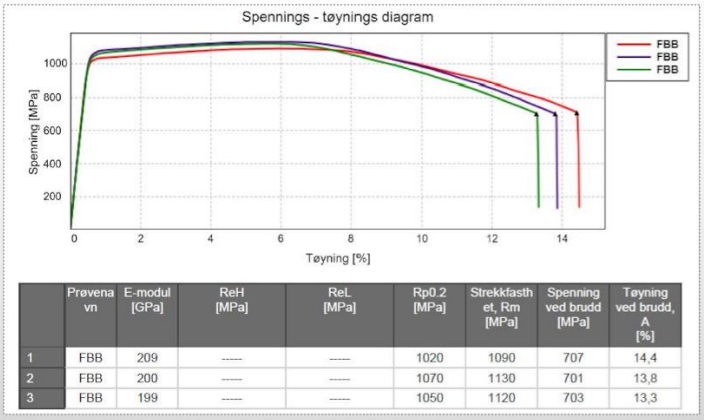

	Prøvenavn	E-modul [GPa]	ReH [MPa]	ReL [MPa]	Rp0.2 [MPa]	Strekkfasthet, Rm [MPa]	Spenning ved brudd [MPa]	Tøyning ved brudd, A [%]
1	FBB	209	-----	-----	1020	1090	707	14,4
2	FBB	200	-----	-----	1070	1130	701	13,8
3	FBB	199	-----	-----	1050	1120	703	13,3

Fig E.2 Tensile result FBB

TENSILE FCB

Office on the web Frame

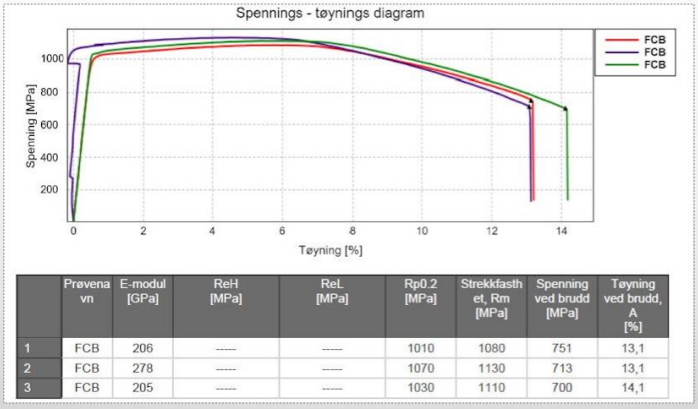

	Prøvenavn	E-modul [GPa]	ReH [MPa]	ReL [MPa]	Rp0.2 [MPa]	Strekkfasthet, Rm [MPa]	Spenning ved brudd [MPa]	Tøyning ved brudd, A [%]
1	FCB	206	-----	-----	1010	1080	751	13,1
2	FCB	278	-----	-----	1070	1130	713	13,1
3	FCB	205	-----	-----	1030	1110	700	14,1

Fig E.3 Tensile result FCB

Appendix F – Fracture surface Preparation

Fig F.1 Before and after etching

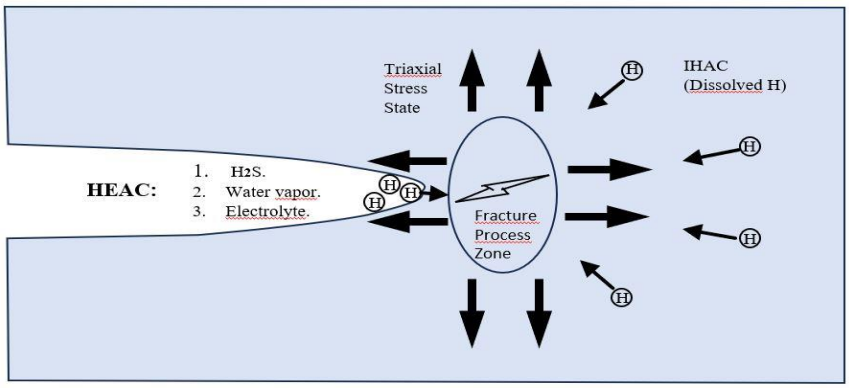

Fig G.1 HEAC/IHAC